

Marine Carbohydrates and Other Sea Spray Aerosol Constituents Across Altitudes in the Lower Troposphere of Ny-Ålesund, Svalbard

Sebastian Zeppenfeld^{1*}, Jonas Schaefer², Christian Pilz², Kerstin Ebell³, Moritz Zeising⁴, Frank Stratmann², Holger Siebert², Birgit Wehner², Matthias Wietz^{4,5,6}, Astrid Bracher^{4,7}, and Manuela van Pinxteren¹

1 Atmospheric Chemistry Department (ACD), Leibniz Institute for Tropospheric Research (TROPOS), Leipzig, Germany

2 Atmospheric Microphysics (AMP), Leibniz Institute for Tropospheric Research (TROPOS), Leipzig, Germany

3 Institute for Geophysics and Meteorology, University of Cologne, Cologne, Germany

4 Alfred Wegener Institute Helmholtz Centre for Polar and Marine Research, Bremerhaven, Germany

5 Max Planck Institute for Marine Microbiology, Bremen, Germany

6 Institute for Chemistry and Biology of the Marine Environment, University of Oldenburg, Oldenburg, Germany

7 Institute of Environmental Physics, University of Bremen, Bremen, Germany

*Correspondence to: Sebastian Zeppenfeld (zeppenfeld@tropos.de)

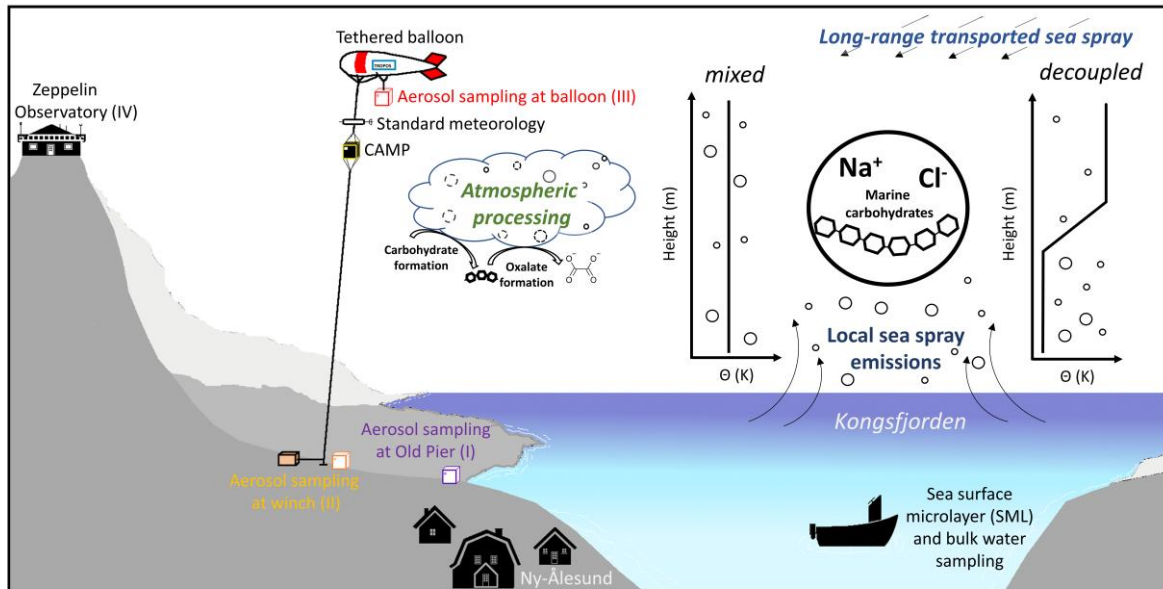
Abstract

Marine combined carbohydrates in aerosol particles (CCHO_{aer}) have the potential to influence cloud formation and properties, but it remains unclear to what extent they reach altitudes relevant for cloud processes. Balloon-borne measurements of major sea spray aerosol (SSA) constituents, including sodium (Na⁺_{aer}) and CCHO_{aer}, were conducted in autumn 2021 and spring 2022 in Ny-Ålesund (Svalbard). Total suspended particles were collected at 321–1112 m, covering both the marine boundary layer and the free troposphere, with Na⁺_{aer} ranging 23–850 ng m⁻³ and CCHO_{aer} 3.8–274 ng m⁻³. The chemical composition of balloon-borne aerosol samples was compared with synchronized ground level measurements at the balloon's winch (Na⁺_{aer}: 35–3710 ng m⁻³; CCHO_{aer}: 1.9–194 ng m⁻³), and at the Old Pier (Na⁺_{aer}: 140–1470 ng m⁻³; CCHO_{aer}: 1.6–10.0 ng m⁻³), where freshly emitted SSA particles were sampled. Surface seawater from the Kongsfjorden was analyzed to evaluate the sea-air transfer of marine CCHO. Air mass histories, atmospheric mixing, and cloud conditions were evaluated for three selected cases to explain vertical concentration patterns. A strong correlation (R=0.78, p<0.001) between combined xylose (<0.2–14.1 ng m⁻³) in CCHO_{aer} and oxalate_{aer} (<1–67 ng m⁻³) across all altitudes, suggests either coproduction or a connection through atmospheric

36 processing. These results provide a first comprehensive picture of local primary sea-air
37 transfer of marine combined carbohydrates and highlight the roles of long-range transport,
38 in-situ formation, and atmospheric processing in shaping their distribution.

39

40



41

42 **1. Introduction**

43 Aerosol particles in the High Arctic atmosphere originate from a complex interplay of primary
44 and secondary emissions from oceanic, terrestrial, cryospheric, and anthropogenic sources,
45 followed by diverse atmospheric processes (Schmale et al., 2021). They play a crucial role in
46 the radiation balance, directly by scattering and absorbing shortwave and longwave radiation,
47 and indirectly by influencing cloud formation and phase state as cloud condensation nuclei
48 and ice-nucleating particles (Lohmann and Feichter, 2005; Penner et al., 2001; Quinn et al.,
49 2015; Yu et al., 2006). These effects are strongly governed by the particles' size distribution
50 and chemical composition (Dusek et al., 2006; Farmer et al., 2015; Kanji et al., 2017; Pilinis et
51 al., 1995).

52 The High Arctic predominantly consists of marine areas, characterized by a seasonally variable
53 extent of sea ice cover and open waters. Consequently, sea spray aerosol (SSA) particles
54 represent a key group of primary aerosol particles in this region (Heutte et al., 2025; Kang et
55 al., 2025; Schmale et al., 2022). As Arctic sea ice coverage continues to decline due to global
56 warming, enhanced by Arctic amplification (Cai et al., 2021; Francis and Wu, 2020; Wendisch
57 et al., 2017, 2023), larger expanses of open ocean are anticipated to become significant
58 sources of SSA emissions (Browse et al., 2014; Struthers et al., 2011). Although direct
59 measurements remain sparse, Sharma et al. (2019) readily observed increasing sea salt
60 aerosol production from sea spray over 34 years at the Arctic air chemistry observatory in
61 Alert, Canada.

62 SSA particles are generated through wind-driven wave action, which causes bubbles at the sea
63 surface to burst, ejecting film and jet droplets into the atmosphere (Veron, 2015). SSA
64 particles primarily consist of inorganic sea salt ions, mainly sodium and chloride, along with
65 organic matter (OM), including significant amounts of marine carbohydrates originating from
66 the sea surface microlayer (SML) and the underlying bulk seawater (Müller et al., 2010; van
67 Pinxteren et al., 2023; Quinn et al., 2015; Russell et al., 2010). In seawater, carbohydrates are
68 produced by photoautotrophic organisms, predominantly as linear or branched oligo- and
69 polysaccharides (Aluwihare et al., 1997; Borch and Kirchman, 1997; Engel and Händel, 2011;
70 Khadem, 2012), collectively referred to as combined carbohydrates (CCHO). They also exist as
71 monosaccharides, known as dissolved free carbohydrates. Both fractions are consumed or
72 transformed by heterotrophic organisms, with turnover rates largely determined by their

73 molecular structure and composition (Arnosti et al., 2021; Engel and Händel, 2011; Ittekkot et
74 al., 1981; Kirchman et al., 2001).

75 Sodium in aerosol particles (Na^+_{aer}) is highly abundant in the marine boundary layer, with only
76 minor terrestrial sources and greater atmospheric stability compared to chloride (Cl^-_{aer}) (Chi
77 et al., 2015; Keene et al., 1986; Manders et al., 2010; Sander et al., 2003). This makes it a
78 valuable conservative tracer for studying the sea-to-air transfer and atmospheric
79 transformation of organic compounds, including marine carbohydrates, as well as other
80 inorganic SSA constituents. Notably, the ratio of OM to Na^+ is significantly higher in SSA
81 particles than in seawater, reflecting not only the preferential enrichment of surface-active
82 substances at the interface but also a more complex interplay of factors such as water
83 solubility, biological activity within the ocean surface, and co-adsorption processes involving
84 matrix constituents (Burrows et al., 2014; Gantt et al., 2011; Hasenecz et al., 2020, 2019;
85 Hoffman and Duce, 1976; Jayarathne et al., 2016; van Pinxteren et al., 2017; Quinn et al., 2015;
86 Russell et al., 2010; Schill et al., 2018). This enrichment is particularly pronounced in
87 submicron particles compared to supermicron particles. Furthermore, following the sea-to-air
88 transfer of OM and CCHO, recent laboratory (Hasenecz et al., 2020; Malfatti et al., 2019) and
89 field (Zeppenfeld et al., 2021, 2023) observations suggest their molecular transformation or
90 additional in-situ formation, driven by abiotic, microbial or enzymatic activities in the
91 atmosphere.

92 SSA particles are known to function as both cloud condensation nuclei (Orellana et al., 2011;
93 Xu et al., 2022) and ice-nucleating particles (Alpert et al., 2022; DeMott et al., 2016; Hill et al.,
94 2023; Mirrielees et al., 2024), underscoring their important role in cloud microphysics, cloud
95 formation, and precipitation processes. Recently, Hartmann et al. (2025) demonstrated,
96 through a combination of lab and field data, that SSA particles' ice-nucleating activity is likely
97 attributable to the polysaccharides they contain. Model simulations further indicated that the
98 ice-nucleating activity of marine polysaccharides is particularly significant within the
99 temperature range between -20 and -15°C in remote oceanic regions, where contributions
100 from terrestrial ice-nucleating particles are minimal or absent. Furthermore, Rocchi et al.,
101 (2024) demonstrated that the presence of glucose-rich CCHO, in combination with sea salt,
102 significantly enhances SSA production in eastern Arctic waters. This finding may improve the
103 predictability of SSA emissions in marine models.

104 In the field, marine combined carbohydrates in aerosol particles (CCHO_{aer}) have been
105 predominantly measured at ship-based or coastal locations, which are in close proximity to
106 local marine emission sources both horizontally and vertically (Leck et al., 2013; van Pinxteren
107 et al., 2023; Zeppenfeld et al., 2021, 2023). In contrast, only a few studies have investigated
108 CCHO_{aer} (Karl et al., 2019; Yttri et al., 2024) at an elevated mountain site in a marine-influenced
109 setting, aiming to assess atmospheric concentrations at higher altitudes. Vertically resolved
110 field data comparing ground-level and elevated altitudes using mobile platforms for marine
111 CCHO_{aer} have, however, been lacking to date. This is due to several methodological challenges,
112 most fundamentally the absence of suitable high-resolution online detection techniques for
113 CCHO_{aer}, reflecting the inherent analytical difficulty of this compound class. As a consequence,
114 current approaches rely on offline analyses, which are further constrained by low atmospheric
115 concentrations that approach their detection limits. In addition, lightweight yet powerful high-
116 flow pumps remain technically challenging to realize for mobile airborne platforms (e.g.,
117 drones or balloon-based systems), where payload and power constraints limit the collection
118 of sufficient aerosol mass during short sampling periods. As a result, it remains unclear to what
119 extent and under which conditions CCHO_{aer} reach the upper marine boundary layer and the
120 free troposphere, leaving high uncertainty about the broader relevance of these biomolecules
121 for cloud formation and glaciation beyond controlled laboratory conditions.

122 Previous airborne measurements around Svalbard (Hara et al., 2003; Simon et al., 2025) and
123 the Canadian Arctic (Köllner et al., 2017) demonstrated that SSA particles, identified by Na⁺
124 and Cl⁻, are present in higher altitudes of the lower troposphere, and, to a lesser extent, reach
125 the middle free troposphere (3–6 km a.s.l.). Some of these aerosol particles showed signs of
126 atmospheric aging, such as the replacement of chloride with nitrate and sulfate in the SSA
127 particles. While vertically resolved data exists for major inorganic SSA constituents, such
128 extended information is lacking for marine CCHO_{aer}.

129 Recent methodological advances now allow for a more detailed investigation of the transport
130 mechanisms and atmospheric chemical fate of marine carbohydrates. In this study, we
131 present atmospheric concentrations of these biomolecules alongside common inorganic SSA
132 constituents. Measurements were conducted from ground level up to various altitudes within
133 the boundary layer and lower free troposphere using a tethered helium balloon in Ny-Ålesund
134 on Svalbard during autumn 2021 and spring 2022. For selected cases, we examined the
135 influence of mixing state, meteorological conditions, and air mass history on the observed

136 aerosol composition. Finally, this study addresses the potential atmospheric processing and
137 transformation of marine carbohydrates, with a focus on their possible contribution to
138 secondary aerosol formation and their implications for atmospheric chemistry and cloud-
139 relevant processes.

140 **2. Methods**

141 This section summarizes the observational and modelling approaches used in this work. It
 142 covers the study area, field sampling, offline and online measurements, supporting datasets,
 143 model calculations, and statistical and visualization methods for data interpretation. An
 144 overview of all relevant parameters and methods is provided in **Table 1**.

145 **Table 1.** Overview of parameters, methods and sample/media types used in this study.

Category	Parameters	Method/Instrument	Sample/Medium
Major inorganic ions	Na ⁺ , K ⁺ , Mg ²⁺ , Ca ²⁺ , Cl ⁻ , SO ₄ ²⁻ , oxalate	Ion chromatography	Bulk seawater, SML, aerosol particles (filter)
Free and combined carbohydrates	Fuc, Rha, Ara, Gal, Glc, Xyl, Man, Fru, GalN, GlcN, MurAc, GalAc, GlcAc	HPAEC-PAD	Bulk seawater, SML, aerosol particles (filter)
Sea surface temperature	SST	Digital Thermometer	Ocean surface
Aerosol number concentration	N ₁₅₀ (150-2900 nm)	POPS (CAMP)	Atmospheric column
Meteorology	T, U, WD, RH, p, wind, θ, q	Standard meteorology package + thermodynamic equations	Atmosphere at ground (AWIPEV), atmospheric column
Cloud properties	Clouds and hydrometer types, IWP, LWP, IWV	Cloudnet + HATPRO	Atmospheric column
Biogeochemistry (model)	TChl-a, dissolved acidic polysaccharides	FESOM2.1-REcoM3	Ocean surface
Air mass origin	48-h back-trajectories	NOAA HYSPLIT	Several altitudes of atmosphere

146

147 **2.1 Study area: Ny-Ålesund as an atmospheric observation site**

148 Ny-Ålesund, located at 78.9°N at the Kongsfjorden in Svalbard (Norway), belongs to the
 149 world's northernmost permanently inhabited settlements with a year-round accessibility. It
 150 serves as a key research site for studying Arctic climate change and Arctic amplification. Ny-

151 Ålesund hosts long-term monitoring sites for aerosols and meteorology, such as the Zeppelin
152 Observatory (Platt et al., 2022), Gruvebadet (Amore et al., 2022), and the AWIPEV Observatory
153 (Maturilli et al., 2013, 2015). These, along with additional research stations operated by
154 various international institutions, provide valuable data for both long-term atmospheric
155 studies and short-term investigations like the present one.

156 However, Ny-Ålesund is not representative of the entire High Arctic. Its distinct topography,
157 situated within a fjord and surrounded by high mountains up to 800 m, leads to complex
158 atmospheric dynamics, including foehn-like effects (Shestakova et al., 2021). The local
159 boundary layer is relatively shallow characterized by an average mixing layer height below
160 700 m and a strong influence by orographic effects (Chang et al., 2017; Dekhtyareva et al.,
161 2018; Gierens et al., 2020). While free-tropospheric winds are predominantly westerly,
162 surface winds result from an interplay of land-sea breeze circulations, southeasterly
163 channeled winds along the fjord axis, and katabatic flows from the Zeppelin mountain range,
164 the Broeggerbreen glacier, or the Kongsvegen glacier (Esau and Repina, 2012; Gierens et al.,
165 2020). Additionally, large wind shear has been observed to generate turbulence, leading to
166 frequent neutral stratification (Gierens et al., 2020). Furthermore, boundary layer mixing can
167 occur even when a positive gradient in potential temperature exists, suggesting more stable
168 stratification. During the present field campaign, we observed that near-surface winds often
169 shift unpredictably, changing direction without a clear pattern, making airflow dynamics
170 challenging to interpret.

171 From an oceanographic perspective, Svalbard is similarly exceptional. The region is influenced
172 by the cold Arctic waters of the Spitsbergen Polar Current and the warm waters of the West
173 Spitsbergen Current (Feltracco et al., 2021). Kongsfjorden, located on the western coast of
174 Spitsbergen, lies at the interface of High Arctic and Atlantic influences, making it a dynamic
175 and variable environment (Bischof et al., 2019).

176 Therefore, findings from Ny-Ålesund may not be fully transferable to atmospheric processes
177 over sea ice or the open ocean in the High Arctic. However, in general, the representativeness
178 of any single Arctic site is highly questionable, as Freud et al., (2017) found significant
179 heterogeneity in aerosol particle size distribution across all Arctic sites in their study.

180 **2.2 Field sampling**

181 The field samples (aerosol particles, bulk seawater and SML) for this study were collected near
182 Ny-Ålesund and from the adjacent Kongsfjorden during autumn 2021 and spring 2022.

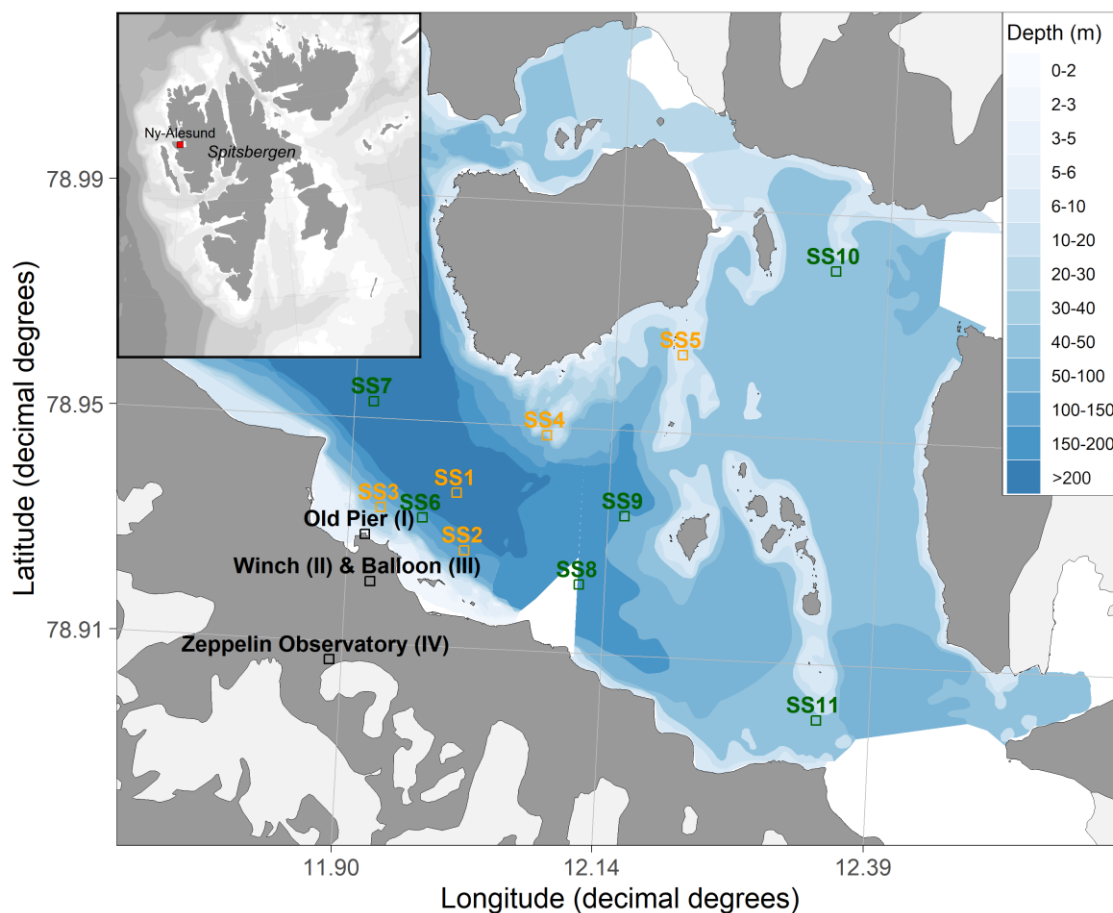


Figure 1. Map of the sampling locations. Aerosol particles were collected at: (I) the Old Pier, representing fresh SSA emissions; (II) the winch, representing ground measurements; (III) the tethered balloon at various altitudes; and (IV) the Zeppelin Observatory, serving as a reference for comparison. Bulk and SML samples were collected from different locations within Kongsfjorden. Orange squares (SS1-SS5) indicate autumn 2021 samples, while green squares (SS6-SS11) represent spring 2022 samples. Blue shading indicates water depth.

183

184 *a) Bulk seawater and SML sampling*

185 In total, 11 bulk surface seawater and 11 SML samples were taken from a small boat at various
186 dates and locations across the Kongsfjorden (**Figure 1, Table S1**). Bulk water samples were
187 obtained from a depth of 1 m using low-density polyethylene (LDPE) bottles secured to a
188 telescopic rod. The corresponding SML samples were collected using the glass plate technique
189 (Cunliffe and Wurl, 2014; van Pinxteren et al., 2012). A glass plate measuring
190 50 cm × 20 cm × 0.5 cm, with an oval sampling area of 2000 cm², was immersed vertically into

191 the surface of the fjord seawater and withdrawn at a steady rate of 15 cm s^{-1} . The SML film
192 attached to the glass surface was drained into a precleaned wide-neck plastic bottle using a
193 funnel and a framed Teflon wiper. Water samples were filtered through $0.2 \text{ }\mu\text{m}$ polycarbonate
194 filters (Whatman® Nuclepore™, 47 mm diameter) to separate dissolved and particulate
195 fractions. The filtrate, filters and field blanks were preserved at -20°C until chemical analyses
196 (inorganic ions, carbohydrates). Sea surface temperature (SST) was measured directly from
197 the boat at a depth of approximately 10 cm using a digital thermometer.

198 *b) Aerosol particle sampling in the surroundings of Ny-Ålesund*

199 Total suspended aerosol particles (TSP) were captured on polycarbonate filters ($0.8 \text{ }\mu\text{m}$,
200 Whatman® Nuclepore™, 47 mm diameter) at four locations (**Figure 1**): (I) Near the Old Pier
201 next to Kongsfjorden (8 samples), representing fresh SSA emissions; (II) near the balloon winch
202 close to the AWIPEV Observatory (17 samples), representing ground measurements; (III) at
203 high altitudes at the tethered balloon (14 samples); and (IV) at the Zeppelin Observatory
204 (1 sample), serving as a reference for comparison. **Table S2** provides details of individual
205 aerosol particle samplings near the Old Pier (I), while **Table S3** presents the sampling times,
206 locations and heights of all the individual high-altitude aerosol samples (III & IV), along with
207 the corresponding simultaneous ground-level samples (II) taken near the winch.

208 For sampling aerosol particles at the Old Pier (4 m above sea level), a filter holder with a
209 polycarbonate filter attached to a pump was used. Sampling lasted between 4 and 7 days.
210 Flow rates, measured at the beginning and the ending of the sampling with a flowmeter,
211 ranged from 5 to 10 L min^{-1} , with total air volumes between 44 and 82 m^3 . The estimated
212 diameter-dependent collection efficiency of this TSP sampling setup, assuming a 90°
213 aspiration angle, is shown in **Figure S1**. To reduce the risk of pump failure due to cold
214 temperatures or snow, the pumps were housed in a Zarges box for protection.

215 High-altitude TSP samples were collected using the helium-filled tethered balloon BELUGA, as
216 described in detail by Pilz et al. (2023). The balloon's altitude was controlled using an electric
217 winch located near the AWIPEV Observatory, with ascent and descent rates from 1 to 3 m s^{-1} .
218 The tethered balloon operated under various meteorological conditions, including both clear
219 and cloudy skies. At a specified altitude, a HALFBAC (High-volume And Light-weight Filter
220 sampler for BALloon-borne appliCation) (Grawe et al., 2023) collected aerosol particles 2-3 m
221 below the balloon. The HALFBAC is a custom-designed, lightweight aerosol particle sampler

222 operating at a pump flow between 25 and 35 L min⁻¹. It is capable of collecting sufficient
223 aerosol mass on filters at high altitudes for subsequent offline chemical and microphysical
224 analyses. Simultaneously, another HALFBAC collected ground-level aerosol particles near the
225 electric winch (20 m above sea level). Additionally, one aerosol sample (Filter ID 62, sampling
226 date: 10/05/2022) was collected at the Zeppelin Observatory, a permanent monitoring station
227 located at 474 m a.s.l. on Zeppelinfjellet, using the HALFBAC. Synchronized aerosol particle
228 sampling at the winch and the balloon typically lasted around two hours, as detailed in **Table**
229 **S3**. The collection efficiency for TSP sampling using HALFBAC is discussed in the supplement
230 (A1) and **Figure S1**.

231

232 **2.3 Chemical analyses from offline aerosol particle filters and seawater**

233 For the analysis of major cations, anions and marine carbohydrates in aerosol particles, the
234 complete polycarbonate filters were extracted in 6-7 mL of ultrapure water
235 (resistivity > 18.2 MΩ) for two hours followed by a filtration through a 0.45 μm syringe filter.
236 Frozen seawater samples were thawed at 4°C in a refrigerator one day before analysis.

237 *a) Major cations and anions*

238 Major inorganic ions, including sodium (Na⁺), potassium (K⁺), magnesium (Mg²⁺), calcium
239 (Ca²⁺), chloride (Cl⁻), sulfate (SO₄²⁻), and oxalate, were quantified in 0.45 μm filtered aqueous
240 aerosol extracts, bulk seawater and SML samples using ion chromatography (Dionex ICS-6000,
241 Thermo Scientific) as described by Zeppenfeld et al. (2021). Cations were separated
242 isocratically with a 36 mM methanesulfonic acid eluent on a Dionex IonPac CS16-4 μm column
243 (2 mm × 250 mm), paired with a Dionex IonPac CG16-4 μm guard column (2 mm × 50 mm).
244 For anion separation, a gradient from 4 to 40 mM KOH was applied on a Dionex IonPac AS18
245 column (2 mm × 250 mm), along with a Dionex IonPac AG18 guard column (2 mm × 50 mm).
246 The analytical uncertainty for each ion was below 5%. Aerosol extracts were measured
247 undiluted, while bulk seawater and SML samples were analyzed at a 1:15,000 dilution.

248 *b) Dissolved free and combined carbohydrates*

249 Carbohydrates in seawater and aerosol particle extracts were measured according to the
250 protocols outlined by Zeppenfeld et al. (2020, 2021), utilizing high-performance anion-
251 exchange chromatography with pulsed amperometric detection (HPAEC-PAD). The system
252 was equipped with a Dionex CarboPac PA20 analytical column (3 mm × 150 mm) and a Dionex
253 CarboPac PA20 guard column (3 mm × 30 mm). The applied eluent gradient separated the
254 following monosaccharide units: fucose (Fuc), rhamnose (Rha), arabinose (Ara), galactose
255 (Gal), glucose (Glc), xylose (Xyl), mannose (Man), fructose (Fru), galactosamine (GalN),
256 glucosamine (GlcN), muramic acid (MurAc), galacturonic acid (GalAc), and glucuronic acid
257 (GlcAc). The analytical uncertainty for each monosaccharide was below 10%. Dissolved free
258 carbohydrates are measured without hydrolysis, whereas CCHO include those
259 monosaccharides released by acid hydrolysis (0.8 M HCl, 100°C, 20 h). For seawater samples,
260 particulate combined carbohydrates (pCCHO, >0.2 µm) were measured from 0.2 µm
261 polycarbonate filters, while dissolved combined carbohydrates (dCCHO, <0.2 µm) were
262 measured from the filtrate after desalination via electrodialysis. Both fractions were later
263 summed to represent the total CCHO. For the winch and balloon samples, the limited air
264 volume and resulting low aerosol mass collected on the filters permitted quantification only
265 of the major monosaccharides (typically Glc, Xyl, Gal, Ara), while minor monosaccharides
266 remained largely below the instrumental detection limits. In contrast, samples from the Old
267 Pier and surface seawater provided sufficient analyte mass to quantify the full suite of the
268 CCHO monosaccharides.

269

270 **2.4 Vertical profiles from online measurements**

271 *a) Size-resolved aerosol particles number concentrations*

272 An optical particles size spectrometer (POPS, Handix), integrated into the Cubic Aerosol
273 Measurement Platform (CAMP) as described by Pilz et al. (2022), provided the integrated total
274 number concentrations (N_{150}) for aerosol particles between 150 and 2900 nm at a temporal
275 resolution of 1 second. On selected dates of HALFBAC sampling, CAMP was operated
276 simultaneously 25 m below the balloon providing insight into the vertical profile of N_{150} during
277 specific events. Vertical profiles are presented as rolling averages over 30 seconds.

278

279 *b) Meteorological observations and calculations*

280 Standard meteorological parameters, including altitude, ambient temperature (T), wind speed
281 (U), wind direction (WD), air pressure (p), and relative humidity (RH), were measured for the
282 elevated-altitude samples using a standard meteorology package positioned approximately
283 20 m below the balloon (Pilz et al., 2023). The potential temperature (θ) within the
284 atmospheric column - as a measure of the static stability of the unsaturated atmosphere - was
285 calculated using Eq. I, where T is the ambient temperature (K), p is the atmospheric pressure
286 (hPa), p_0 is the reference pressure (1000 hPa), R is the specific gas constant ($287 \text{ J kg}^{-1} \text{ K}^{-1}$) and
287 c_p is the specific heat capacity of dry air at constant pressure ($1004 \text{ J kg}^{-1} \text{ K}^{-1}$).

$$288 \quad \theta = T \left(\frac{p_0}{p} \right)^{\frac{R}{c_p}} \quad (\text{Eq. I})$$

289 Specific humidity (q)–remaining constant during adiabatic ascent or descent as long as no
290 phase changes occur–was calculated using Eq. II from Egerer et al. (2021), where R_d/R_v (the
291 ratio of specific gas constants for dry air and water vapor) is approximately 0.622, and $e_s(T)$
292 represents the temperature-dependent saturation vapor pressure.

$$293 \quad q = \frac{R_d/R_v \cdot e_s(T) \cdot RH}{p - (1 - R_d/R_v) \cdot e_s(T) \cdot RH} \quad (\text{Eq. II})$$

294 Meteorological data measured 2 m above the ground (13 m above sea level) at the AWIPEV
295 Atmospheric Observatory (Maturilli, 2020), represented the weather conditions during
296 aerosol sampling at the winch.

297 **2.5 Supporting observations and model calculations**

298 Major inorganic ions measured at the Zeppelin Observatory with a 24-hour resolution using a
299 statically installed aerosol sampler (Filter_3pack) as part of the European Monitoring and
300 Evaluation Programme (Tørseth et al., 2012) by the Norwegian Polar Institute (NPI) and the
301 Norwegian Institute for Air Research (NILU) were obtained from the EBAS database for the
302 study duration (Aas et al., 2022, 2023). The Filter_3pack data were utilized in two ways:

303 1. **Comparing sampling techniques:** Data from the Filter_3pack were compared with one
304 HALFBAC aerosol particle sample collected directly at the Zeppelin Observatory (Filter
305 ID 62, 10 May 2022) to evaluate potential artifacts arising from differences in sampling
306 techniques and filter media. Despite variations in time resolution and methods,
307 sodium, potassium, chloride, and sulfate concentrations showed strong agreement
308 (detailed in the supplement A2 and **Figure S2**).

309 2. **Comparison with balloon data:** Sodium concentrations measured at the Zeppelin
310 Observatory were directly compared with those obtained from the tethered balloon
311 sampling.

312 Information on the occurrence of clouds and hydrometeor types at Ny-Ålesund were taken
313 from the Cloudnet classification product (Illingworth et al., 2007; Nomokonova et al., 2019),
314 which is based on a combination of ground-based cloud radar, ceilometer, and numerical
315 weather prediction output. Vertically integrated ice water content (IWC), i.e. ice water path
316 (IWP), has been calculated from the Cloudnet IWC product following Hogan et al. (2006).
317 Vertically integrated cloud liquid water (liquid water path; LWP) and water vapor (IWV) were
318 taken from zenith HATPRO microwave radiometer measurements (Nomokonova et al., 2019).

319 The 48-hour back-trajectories for the aerosol sampling periods were generated using the
320 NOAA HYSPLIT model (Stein et al., 2015). Trajectories were calculated hourly based on GDAS1
321 meteorological data (Global Data Assimilation System; 1° spatial resolution; 3-hour intervals)
322 for various arrival heights: 50 m (ground level), 474 m (Zeppelin Observatory), and the specific
323 balloon sampling altitudes. Sea ice concentration data were obtained from the NOAA-
324 maintained ERDDAP server (Environmental Research Division's Data Access Program). The
325 back-trajectories were used to assess the relative influence of distant sources, such as the
326 marginal ice zone, versus local ice-free oceanic emissions on the aerosol chemical
327 composition. Given the rather short atmospheric residence time of supermicron SSA particles

328 (Madry et al., 2011; Veron, 2015), which account for most of the SSA mass in TSP, and the
329 increasing uncertainties associated with longer back-trajectory periods, we considered a 48-
330 hour back-trajectory length appropriate for this analysis.

331 Ocean surface concentrations for total chlorophyll a (TChl- a) and dissolved acidic
332 polysaccharides were obtained by a coupled setup of the ocean sea ice biogeochemistry
333 model FESOM2.1-REcoM3 (Gürses et al., 2023), to which additional state equations have been
334 added to simulate dissolved and particulate organic carbon following Engel et al. (2004) and
335 Schartau et al. (2007). The simulation was set up following Gürses et al. (2023) and using the
336 Arctic-specific tuning of Oziel et al. (2022). The modelled dissolved acidic polysaccharides were
337 used as a proxy for dCCHO. Although they represent only a fraction of dCCHO, their
338 concentrations were shown to be within the same order of magnitude as field observations
339 (Zeising et al., 2026). Monthly model output was obtained on an irregular grid with
340 approximately 4.5 km resolution in the Arctic Ocean. This configuration has already been
341 applied successfully in Leon-Marcos et al. (2025).

342

343 **2.6 Statistics, data processing, visualization and text optimization**

344 Statistical analyses, calculations and visualization were conducted using OriginPro 2024,
345 Microsoft Excel, IDL, python3 and R version 4.2.1 with the ncd4 (Pierce, 2023), openair
346 (Carslaw and Ropkins, 2012), reshape2 (Wickham, 2007), scales (Wickham et al., 2023b),
347 lubridate (Grolemund and Wickham, 2011), cmocean (Thyng et al., 2016), maps (Brownrigg,
348 2023), mapdata (Brownrigg, 2013), rgdal (Bivand et al., 2022), raster (Hijmans, 2023),
349 RColorBrewer (Neuwirth, 2022), sp (Bivand et al., 2013), dplyr (Wickham et al., 2023a), ggplot2
350 (Wickham, 2016), and PlotSvalbard (Vihtakari, 2020) packages. Box-and-whisker plots
351 illustrate the interquartile range (box), the median (horizontal line inside the box), the mean
352 (open square), the minimum and maximum values (whiskers). Text and language were
353 optimized using Open AI's ChatGPT-4 Turbo.

354 **3. Results and Discussion**

355 **3.1 Chemical constituents in marine aerosol particles from their oceanic source** 356 **to elevated altitudes**

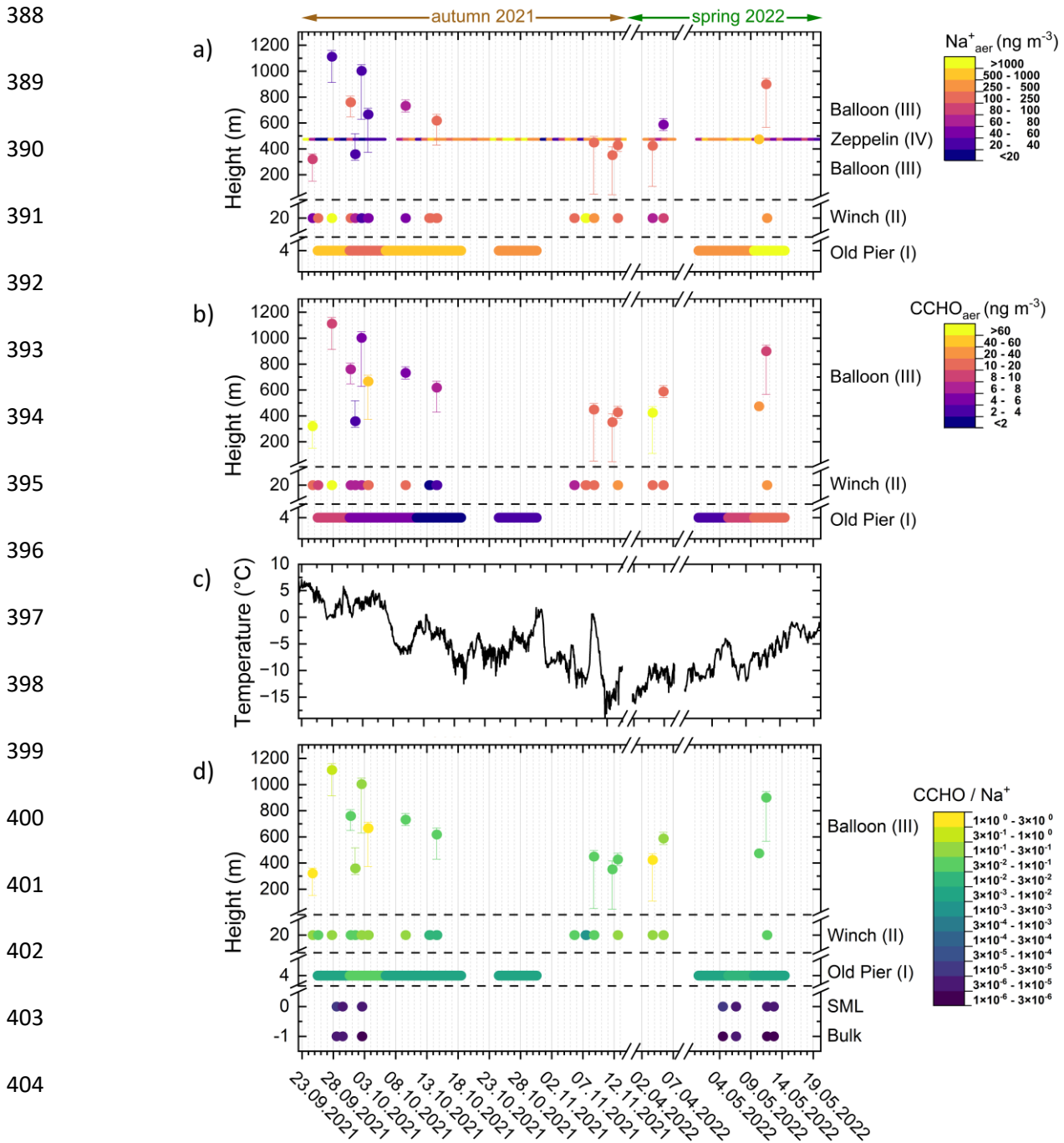
357 *Sodium in aerosol particles (Na^+_{aer})*

358 Sodium, a dominant and chemically stable component of SSA, is commonly used as a tracer
359 for tracking ocean-derived emissions in atmospheric studies (Manders et al., 2010; van
360 Pinxteren et al., 2017; White, 2008). In this study, consistently high Na^+_{aer} concentrations were
361 observed on the TSP filters at the Old Pier next to Kongsfjorden in both autumn 2021 and
362 spring 2022 (**Figure 2a**), ranging from 140 to 1470 ng m^{-3} (median: 495 ng m^{-3} ; $n=8$). The area
363 around Ny-Ålesund, especially the Old Pier, remained largely ice-free, indicating a negligible
364 influence of local sea ice on SSA emissions.

365 Na^+_{aer} at the winch site, located further inland but still at ground level (35–3710 ng m^{-3} ;
366 median: 155 ng m^{-3} ; $n=17$), and at the balloon (321–1112 m; 23–850 ng m^{-3} ; median:
367 124 ng m^{-3} ; $n=15$) was generally lower than at the Old Pier, though episodic high events
368 occurred at all sites. This wide variability from low ng m^{-3} to a few $\mu\text{g m}^{-3}$ agrees with
369 observations from other marine environments and altitudes (Fomba et al., 2014; Li et al.,
370 2024; Ooki et al., 2002; Theodosi et al., 2010; Triesch et al., 2021; Zeppenfeld et al., 2021,
371 2023).

372 Since winch and balloon sampling were always synchronized, direct comparisons were
373 possible (**Figure 3**). Several events showed nearly identical Na^+_{aer} concentrations (winch vs.
374 balloon), e.g., 30 Sep: 191 vs. 207 ng m^{-3} ; 2 Oct: 35 vs. 36 ng m^{-3} ; 9 Oct: 59 vs. 60 ng m^{-3} ; 12
375 Nov: 240 vs. 223 ng m^{-3} . In contrast, other periods exhibited strong vertical gradients with
376 higher ground-level concentrations (e.g., 27 Sep: 1840 vs. 23 ng m^{-3} ; 5 Apr: 84 vs. 54 ng m^{-3} ;
377 11 May: 496 vs. 125 ng m^{-3}), while two cases showed higher values at the balloon (24 Sep: 47
378 vs. 99 ng m^{-3} ; 3 Apr: 77 vs. 194 ng m^{-3}). These variations are likely driven by atmospheric
379 processes, including dry and wet deposition (Farmer et al., 2021), dilution during vertical and
380 horizontal transport from the emission region (Wong et al., 2019), vertical mixing (Pilz et al.,
381 2024) and differing air mass histories (Willis et al., 2018), which will be examined in detail for
382 three selected cases later in this study.

383 Na^+_{aer} at the Zeppelin Observatory largely agreed with the balloon measurements (56–213%
 384 overall; 92–107% in five events; **Table S6**), despite differences in time resolution (24 h vs. 1–
 385 2 h), sampling altitude, the horizontal distance between the sites, Svalbard’s complex
 386 topography (Gierens et al., 2020; Shestakova et al., 2021), and the fact that meteorological
 387 conditions and atmospheric mixing states have not yet been considered.



388
 389
 390
 391
 392
 393
 394
 395
 396
 397
 398
 399
 400
 401
 402
 403
 404
 405
 406
 407

Figure 2. Time-resolved atmospheric concentrations of a) Na^+_{aer} and b) CCHO_{aer} in aerosol particles (TSP) collected in autumn 2021 and spring 2022 in Ny-Ålesund at several heights (m a.s.l.) from four sites: Old Pier, winch near the AWIPEV Observatory, balloon and the Zeppelin Observatory. Dots represent the median height during the total sampling time and vertical error bars represent maximum and minimum height of the sampler during the active sampling. The x-axis ticks represent the start of each date at midnight. c) Air temperature (2 m above ground) measured at the AWIPEV Observatory. d) CCHO/Na^+ ratios within the bulk seawater, the SML and in the aerosol particles at several heights. In panel (a), the label “Balloon (III)” appears twice because balloon sampling for sodium measurements occurred both below and above the fixed altitude of the Zeppelin Observatory.

408 Overall, Na^+_{aer} was detectable up to 1100 m altitude, sometimes at levels comparable to those
 409 near the emission source, indicating effective vertical mixing or transport to cloud-relevant
 410 heights via advection. This vertical distribution is consistent with the aircraft-based SSA
 411 measurements reported by Hara et al. (2003) and Köllner et al. (2017). Longer atmospheric
 412 residence increases the exposure of SSA particles to processing, which can alter their impact
 413 on cloud formation. While Na^+_{aer} is considered chemically stable, co-emitted OM including
 414 carbohydrates may undergo physical, chemical and microbial changes (Zeppenfeld et al.,
 415 2021, 2023). This aspect will be explored further in section 3.3.

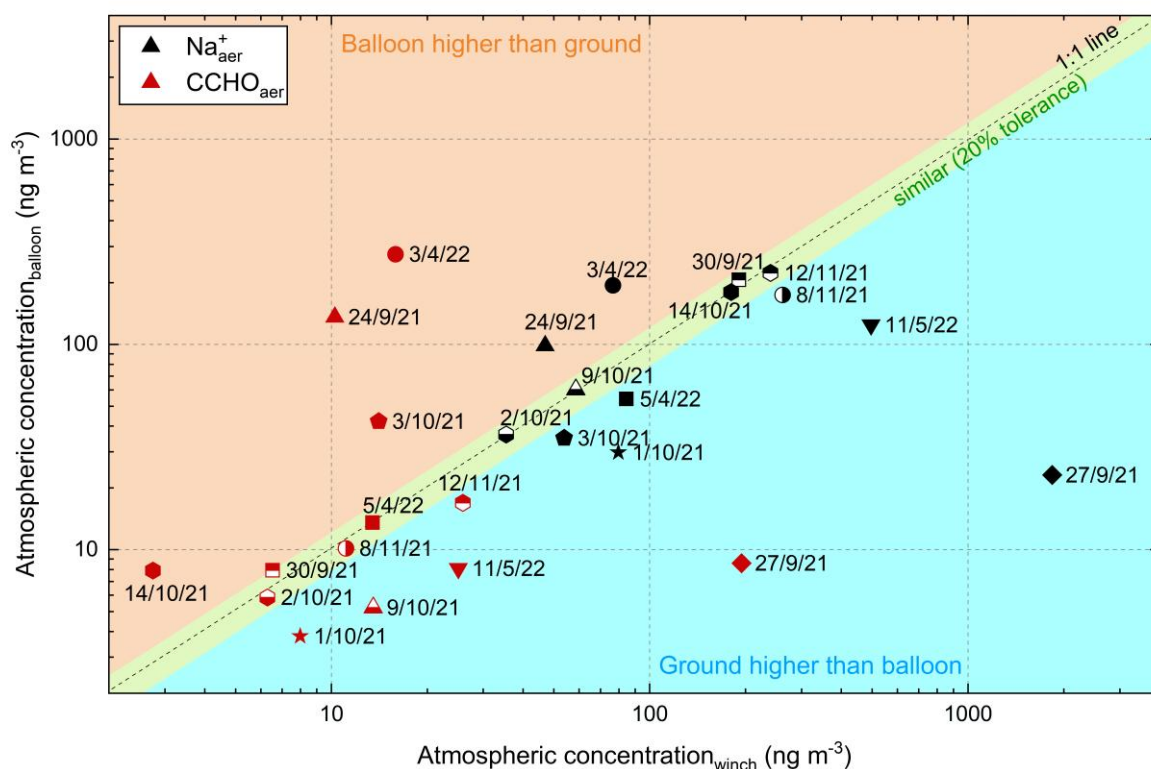


Figure 3. Scatter plot showing Na^+_{aer} (black symbols) and CCHO_{aer} (red symbols) concentrations in TSP measured at the winch, and balloon levels. Marker shapes and fill styles serve as identifiers linking corresponding Na^+_{aer} and CCHO_{aer} values from the same sample. Data points are categorized to indicate whether values were similar, higher at the balloon, or higher at the ground.

416

417

418

419

420 ***Combined carbohydrates in fresh SSA and surface seawater***

421 Similar to sodium, CCHO_{aer} were detected at all sites and altitudes (**Figure 2b**). At the Old Pier,
422 CCHO_{aer} concentrations ranged from 1.6 to 10.0 ng m⁻³ (median: 5.0 ng m⁻³; n=8), showing a
423 seasonal pattern with the highest values at the beginning (end of September 2021) and end
424 (mid of May 2022) of the study period, and lower values in October 2021, coinciding with low
425 air temperatures (**Figure 2c**). No samples were collected between November and April, so
426 winter trends remain unknown.

427 A seasonal trend was also observed for dCCHO in Kongsfjorden seawater. Concentrations
428 peaked in late September/early October and were substantially lower in early to mid-May,
429 averaging only about 50% of the autumn values (**Figure 4**). Most monosaccharides in bulk
430 dCCHO showed a strong co-variation with SST ($R^2= 0.79-0.93$; n = 11). This relationship was
431 weaker for xylose ($R^2_{\text{Xyl-SST}} = 0.62$) and glucose ($R^2_{\text{Glc-SST}} = 0.53$) in bulk dCCHO, and generally
432 more moderate in the SML for most monosaccharides (**Figure 4**).

433 In contrast, pCCHO as a whole showed no clear seasonal trend in seawater (**Figure S3**).
434 However, a few monosaccharides within bulk water pCCHO, in particular fucose, glucosamine,
435 and galactosamine, displayed a moderate correlation with SST ($R^2_{\text{Fuc-SST}} = 0.73$; $R^2_{\text{GalN-SST}} =$
436 0.39 ; $R^2_{\text{GlcN-SST}} = 0.69$; n=11). While dCCHO in bulk water exhibited relatively low spatial and
437 intra-seasonal variability, pCCHO and SML samples were considerably more variable, even
438 among samples from the same season (**Figure S4**). This likely reflects the rapid dynamics of
439 pCCHO in relation to phytoplankton blooms (Becker et al., 2020; Engel et al., 2012; Fabiano et
440 al., 1993), as well as the formation of transparent exopolymer particles (TEP) from dCCHO in
441 turbulent waters and vertical transport of pCCHO via sedimentation (e.g., as marine snow) or
442 its accumulation in the SML depending on buoyancy (Burns et al., 2019; Engel, 2004; Robinson
443 et al., 2019a, b; Wurl and Holmes, 2008). The SML, in particular, may be more sensitive to
444 these dynamics than the bulk water, potentially explaining its greater fluctuations.

445

446

447

448

449

450

451

452

453

454

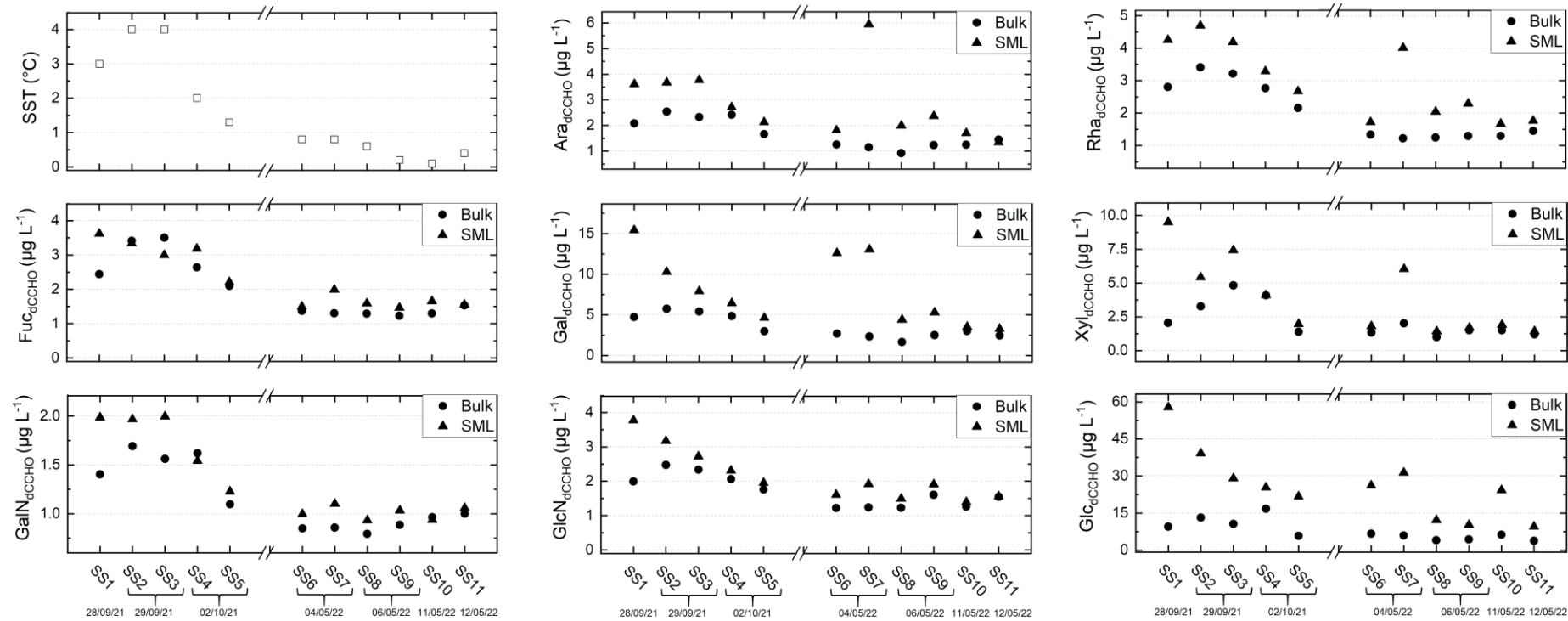


Figure 4. Concentration of measured monosaccharide units in dCCHO from bulk and SML samples collected in Kongsfjorden during autumn 2021 and spring 2022, along with SST measurements taken from bulk samples at the time of sampling.

455 By comparison, dCCHO in bulk water, like dissolved organic carbon (Hansell, 2013; Keene et
456 al., 2017), is likely dominated by recalcitrant and semi-recalcitrant compounds, while the labile
457 fraction is rapidly consumed by heterotrophic bacteria (Goldberg et al., 2011). Notably,
458 combined glucose showed high variability in both dCCHO and pCCHO, likely due to being the
459 main constituent of abundant storage macromolecules such as laminarin (Becker et al., 2020),
460 whose production and turnover may be enhanced during periods of photosynthetic overflow
461 (Barthelmeß et al., 2025), as well as its relatively rapid microbial utilization (Kharbush et al.,
462 2020).

463 The seasonal variation of CCHO_{aer} at the Old Pier may be linked to the seasonal dynamics of
464 marine CCHO in the surface waters of Kongsfjorden, the only local emission source of SSA.
465 These dynamics are likely driven by seasonal shifts in primary production and phytoplankton
466 composition (Assmy et al., 2023; Mayot et al., 2018, van de Poll et al., 2021).

467 Overall, CCHO_{aer} and selected seawater dCCHO monosaccharides showed a broadly consistent
468 seasonal tendency, with elevated values in late summer/early autumn. However, the spring
469 conditions (May) deviate from this pattern, with CCHO_{aer} showing a secondary maximum that
470 is not reflected in seawater dCCHO, where concentrations remain substantially lower. This
471 indicates that the seasonal coupling between (bulk) seawater CCHO and CCHO_{aer} is strongest
472 in late summer/early autumn, while additional processes such as SML enrichment or
473 atmospheric processing may also contribute to the spring aerosol signal.

474 In conclusion, the seasonal variation of CCHO_{aer} measured at the Old Pier is partly consistent
475 with marine carbohydrates in Kongsfjorden seawater, suggesting that surface CCHO is an
476 important but not exclusive source of freshly emitted CCHO_{aer}.

477 ***CCHO_{aer} at the winch and higher altitudes***

478 CCHO_{aer} at the winch site (1.9–194 ng m⁻³; median: 10.6 ng m⁻³; n=17) and at the balloon (3.8–
479 274 ng m⁻³; median: 10.2 ng m⁻³; n=15), showed broader ranges and significantly higher
480 median and maximum values than at the Old Pier (**Figure 2b**), suggesting sources beyond
481 primary sea-air transfer. Unlike the Old Pier, no clear seasonal pattern or altitude dependence
482 was observed, likely due to the winch site's inland location, making it more sensitive to wind
483 direction and changing weather. Also, the higher temporal resolution of the samples likely

484 captured short-term fluctuations rather than integrated seasonal trends. In addition,
485 atmospheric processing during transport and the lack of true winter samples may have further
486 obscured any clear seasonal signal.

487 Similar to sodium, some events (**Figure 3**) showed comparable CCHO_{aer} at the winch and
488 balloon (e.g., 30 Sep: 6.5 vs. 8.0 ng m⁻³; 2 Oct: 6.3 vs. 5.8 ng m⁻³; 8 Nov: 11.1 vs. 10.2 ng m⁻³),
489 while on other dates, concentrations were markedly lower at higher altitudes (e.g., 27 Sep:
490 194 vs. 8.6 ng m⁻³; 11 May: 25 vs. 8.1 ng m⁻³), or conversely, higher aloft (e.g., 24 Sep: 10.2 vs.
491 136 ng m⁻³; 3 Apr: 15.9 vs. 275 ng m⁻³). In most cases, CCHO_{aer} covaried with sodium except on
492 03 Oct, when Na⁺_{aer} was slightly higher at the ground (54 vs. 35 ng m⁻³), whereas CCHO_{aer} was
493 higher at the balloon (42 ng m⁻³) than at the winch (14 ng m⁻³).

494 To investigate oceanic emission and the atmospheric fate of marine CCHO, CCHO/Na⁺ ratios
495 were calculated for all aerosol, bulk seawater and SML samples, representing the primary
496 sources of the SSA particle constituents studied here (**Figure 2d**). Bulk seawater showed the
497 lowest ratios (2.0×10^{-6} – 6.0×10^{-6}) with minimal variability, while the SML had slightly higher
498 ratios (3.3×10^{-6} – 2.5×10^{-5}) due to CCHO enrichment. Specifically, the enrichment factors
499 (EF_{SML}) ranged 1.3 – 4.1 for dCCHO and 0.9 – 6.8 for pCCHO (**Figure S4**), which aligns well with
500 previous studies (Engel and Galgani, 2016; Gao et al., 2012; Zäncker et al., 2021; Zeppenfeld
501 et al., 2021, 2023).

502 At the Old Pier, where fresh SSA was sampled, the ratios were significantly higher (6.2×10^{-3}
503 – 3.3×10^{-2}) indicating the chemo-selective sea-air transfer that enriches surface-active
504 organics relative to sodium in aerosol particles (Hasenecz et al., 2020, 2019; Jayarathne et al.,
505 2016; Schill et al., 2018; Zeppenfeld et al., 2021, 2023). The enrichment effect is typically more
506 pronounced in submicron particles, which have a higher relative contribution of organics than
507 inorganic ions (Quinn et al., 2015). In contrast, supermicron particles are predominantly
508 composed of sea salts, although organic substances are still notably enriched compared to the
509 surface seawater. As total suspended particles were measured here, and most SSA mass
510 resides in the supermicron range (Facchini et al., 2008; O'Dowd et al., 1997), our results
511 primarily reflect supermicron aerosol composition.

512 At the winch sampling station, located at ground level but further inland, the CCHO/Na⁺ ratios
513 in TSP ranged from 2.9×10^{-3} to 2.6×10^{-1} , similar or slightly higher than at the Old Pier. In
514 contrast, balloon samples from elevated altitudes showed higher ratios (3.9×10^{-2} – 1.4×10^0),

515 likely due to depletion of salt-rich supermicron particles during dry and wet deposition (Croft
516 et al., 2009; Hoppel et al., 2002; O'Dowd and de Leeuw, 2007), increasing the relative
517 contribution of OM-dominated submicron particles. Furthermore, the increasing absolute
518 concentration of CCHO at higher altitudes (**Figure 2b**) suggests an atmospheric formation
519 process contributing to the elevated CCHO/Na⁺ ratios, potentially linked to microbial activity
520 in the atmosphere (see section 3.3). However, because only the major monosaccharides
521 (typically Glc, Xyl, Gal, Ara) could be quantified reliably in the winch and balloon samples,
522 relative CCHO compositions were not assessed across the entire vertical sample set.
523 Therefore, they were not used to further substantiate this conclusion, as it has been done in
524 Zeppenfeld et al. (2021, 2023).

525 The CCHO/Na⁺ ratios observed at the Old Pier and the Winch closely align with ship-based
526 measurements from the PASCAL cruise (May–July 2017) in the Fram Strait, Barents Sea, and
527 central Arctic Ocean (Macke and Flores, 2018; Wendisch et al., 2018), where values ranged
528 from 2×10^{-3} to 2×10^{-1} in PM₁₀ based on summed Berner impactor stages (Zeppenfeld et al.,
529 2023). In contrast, the very high CCHO/Na⁺ values ($>1 \times 10^0$) observed at some elevated
530 altitudes in this study were reported only occasionally for submicron particles (0.14–0.42 μm)
531 during PASCAL. This may support the idea that supermicron particle deposition caused the
532 shift in balloon sample ratios, though microbial contributions in the atmosphere are also
533 possible. Moreover, these ratios far exceed those from the Southern Ocean near the western
534 Antarctic Peninsula (8×10^{-4} to 7×10^{-3}) (Zeppenfeld et al., 2021), likely due to differences in
535 surface seawater productivity.

536 Overall, it can be concluded that both Na⁺_{aer} and CCHO_{aer} are transported from the marine
537 emission source to elevated heights within the lower troposphere. In the following section,
538 we discuss the role of meteorological conditions and atmospheric mixing in linking ground-
539 based and balloon-based samples.

540 **3.2 Impact of meteorological conditions on SSA particle constituents in higher**
 541 **altitudes**

542 To examine how meteorological conditions and atmospheric mixing influence Na^+_{aer} and
 543 CCHO_{aer} at high altitudes, three distinct cases with constant weather conditions were selected
 544 (**Figure 5**). These conditions allow for a detailed interpretation of the observed chemical
 545 values.

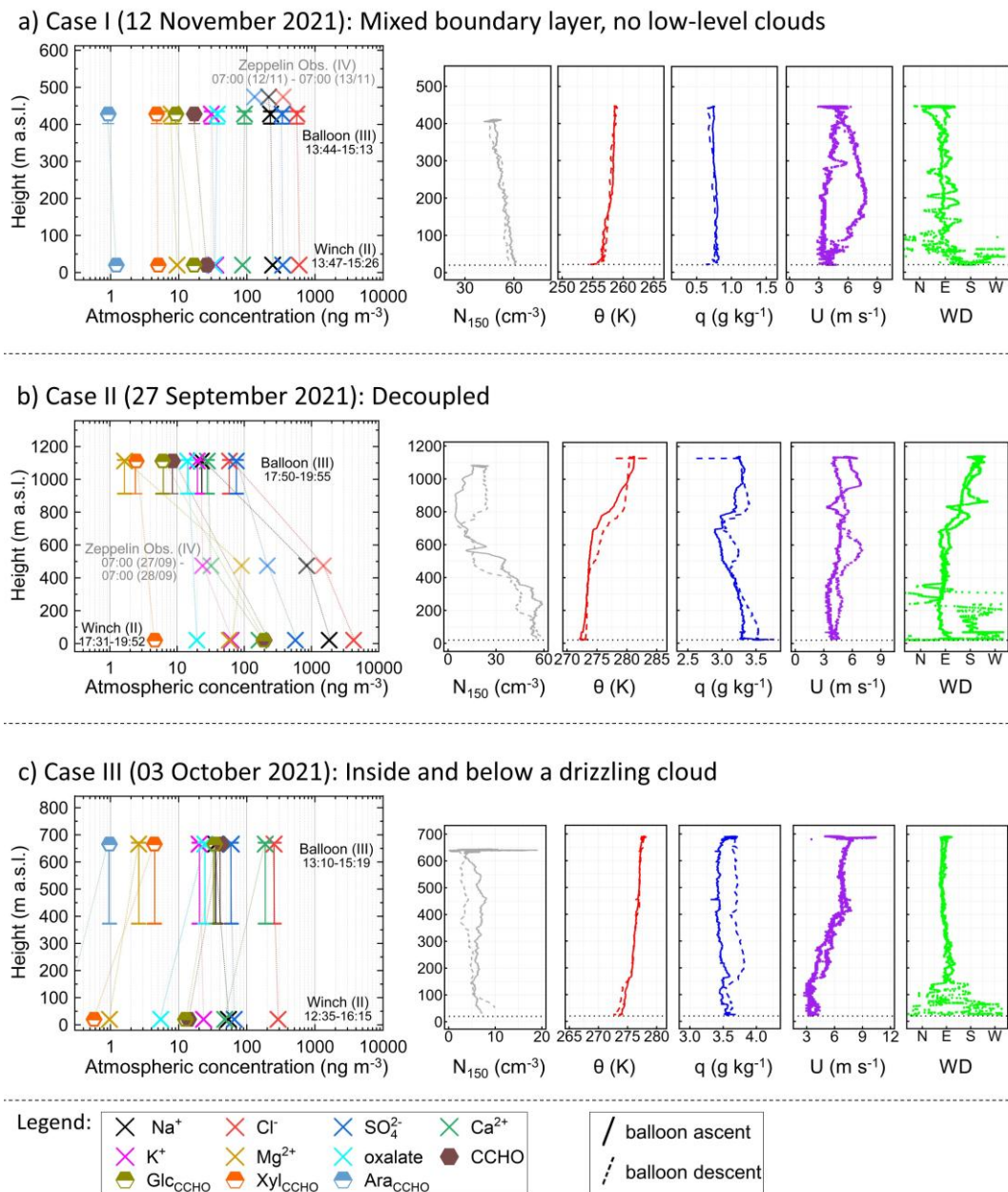


Figure 5. Vertical profiles of three atmospheric cases showing mass concentrations of chemical constituents (inorganic ions, oxalate, total CCHO_{aer} , and major monosaccharides within CCHO_{aer}) in aerosol particles, measured on the ground (winch) and aloft (balloon) using offline filters. Vertical error bars indicate the range between minimal and maximal heights during active sampling at the balloon, while the symbols denote the median sampling heights. Data from the Zeppelin Observatory are also included when available and above detection limits, albeit with a 24-hour resolution. Dotted lines are included to aid in reading the vertical distribution of individual chemical substances. These profiles are complemented by aerosol particle number concentrations of particles bigger than 150 nm (N_{150}), potential temperature (θ), specific humidity (q), wind speed (U), and wind direction (WD) measured during the ascents (solid lines) and descents (dashed lines) of the balloon.

546 To assess atmospheric stability and layering in these cases, vertical profiles of potential
 547 temperature were utilized. To further confirm aerosol mixing conditions, additional
 548 meteorological parameters (specific humidity, wind speed and direction), vertical aerosol
 549 particle number concentrations of particles larger than 150 nm (N_{150}) (**Figure 5**), cloud
 550 conditions (**Figure S5**) and back-trajectory analyses (**Figure 6**) were considered. The selected
 551 cases include (a) a cloud-free mixed boundary layer (12 Nov 2021), (b) a free troposphere
 552 decoupled from the ground (27 Sep 2021), and (c) a boundary layer capped by precipitating
 553 clouds (03 Oct 2021).

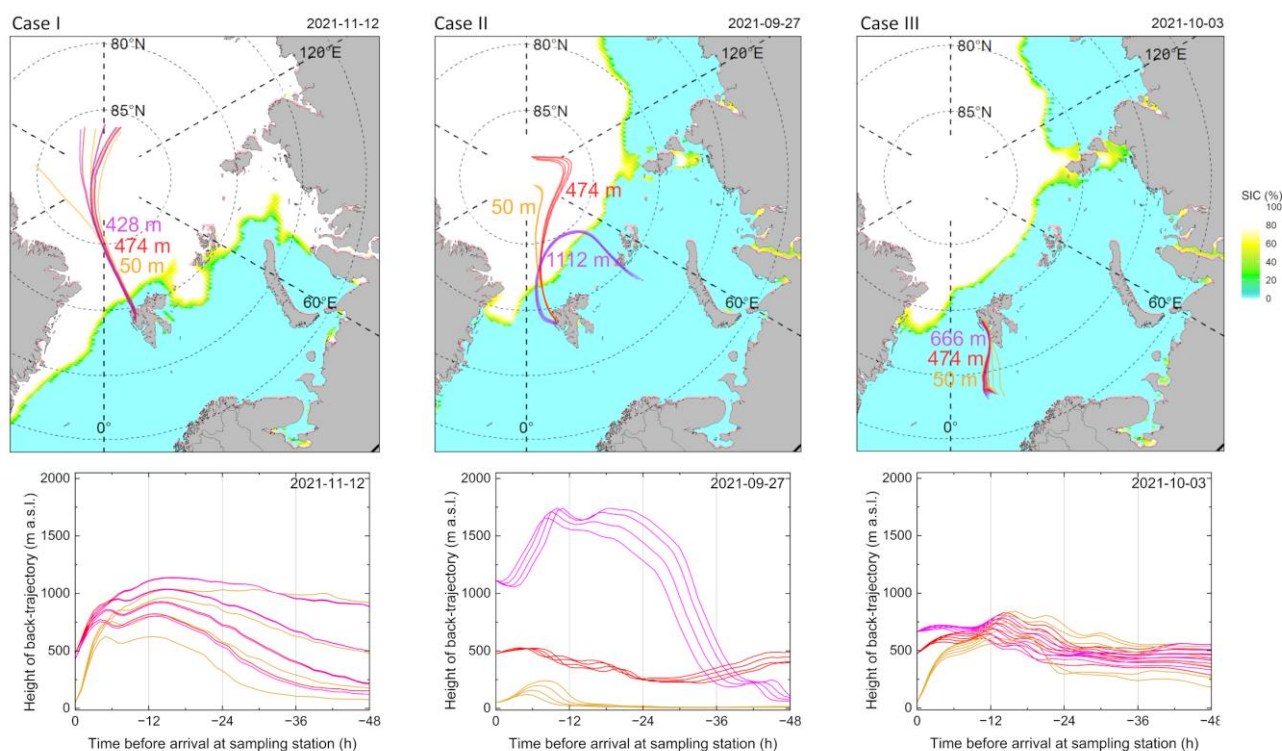


Figure 6. 48-hour back-trajectories calculated on an hourly basis for three arrival heights: orange (50 m, ground-level air masses), red (474 m, height of the Zeppelin Observatory), and purple (variable arrival height, high-altitude air masses sampled at tethered balloon). These are accompanied by daily sea ice concentration (SIC) maps (top) and height profiles (bottom) for three selected aerosol particle sampling cases.

554 **Case I: Mixed boundary layer & no low-level clouds**

555 On 12 November 2021, during the polar night, two HALFBACs were operated simultaneously
 556 at the ground and the balloon (median altitude of 428 m) for approximately 90 min. Ground-
 557 level conditions were -16.7°C , 69% RH, and 1.5 m s^{-1} wind mainly from the southwest. At the
 558 balloon, sampling occurred at a similar temperature (-17.5°C) and RH (72%), but higher wind
 559 speeds (4.3 m s^{-1}) from the northeast to southeast. With $\text{IWV} < 3\text{ kg m}^{-2}$, the atmosphere was
 560 very dry (**Figure S5a**), and only a thin mixed-phase cloud layer at 4.5–5 km altitude was

561 present, with negligible LWP and IWP (**Figure S5a**), unlikely to affect aerosol chemistry within
562 the boundary layer.

563 During the balloon's ascent, potential temperature increased from 255 K to 258 K, with the
564 strongest gradient near the ground. Using the wind speed profile and the Richardson number
565 approach (Akansu et al., 2023), a very shallow surface mixing layer of ~12 m was estimated,
566 likely caused by recent surface cooling. Although this surface inversion and the slightly stable
567 to near-neutral stratification above would limit instantaneous vertical mixing, surface mixing
568 layer height reflects only momentary conditions, whereas aerosol and humidity profiles
569 integrate mixing over longer timescales. The coupling state at the time of measurement is
570 therefore not a reliable indicator of the effective boundary-layer mixing state. Furthermore,
571 as noted in Section 2.1, Ny-Ålesund's complex orography can induce localized turbulent mixing
572 even under stable stratification. In addition, a low-level jet observed during descent, with wind
573 speeds at least 2 m s⁻¹ higher than above and below, provided a significant additional source
574 of turbulence and vertical mixing within the boundary layer (Egerer et al., 2023).

575 At the ground, N₁₅₀ was around 60 cm⁻³, and gradually decreased to 45 cm⁻³ at the balloon's
576 sampling height, indicating a fairly uniform aerosol distribution dominated by primary
577 emissions. Combined with nearly constant specific humidity (~0.7–0.8 g kg⁻¹), a slight wind
578 speed increase with altitude, the low-level jet during descent, and consistent wind direction
579 (**Figure 4a**), these suggest a largely well-mixed boundary layer. HALFBAC samples from ground
580 and balloon showed similar concentrations of inorganic ions (Na⁺_{aer}: 240 & 223, Cl⁻_{aer}: 586 &
581 543, SO₄²⁻_{aer}: 336 & 330, Ca²⁺_{aer}: 87 & 92, Mg²⁺_{aer}: 9.5 & 7.8, K⁺_{aer}: 34 & 30 ng m⁻³), oxalate_{aer}
582 (34 & 37 ng m⁻³), and major CCHO-bound monosaccharides (Glc_{CCHO,aer}: 17 & 9.1, Xyl_{CCHO,aer}:
583 5.0 & 4.7, Ara_{CCHO,aer}: 1.2 & 0.9 ng m⁻³), supporting a well-mixed layer. Despite diverse sources
584 (SSA, dust, anthropogenic, secondary), vertical aerosol composition remained uniform.
585 Zeppelin Observatory 24 h measurements of Na⁺_{aer}, Cl⁻_{aer}, and SO₄²⁻ showed slightly lower
586 concentrations but agreed with balloon results.

587 Back-trajectory analysis revealed that air masses at ground level, the balloon, and Zeppelin
588 Observatory (**Figure 6, Case I**) followed the same path during the 48 hours before sampling.
589 Originating from the Arctic pack ice, they crossed the marginal ice zone with a short residence
590 time before passing over the ice-free ocean and Kongsfjorden, where most SSA compounds
591 were likely taken up. The back-trajectory heights indicate a vertical connection between the

592 three air masses, confirming a similar transport history, influenced by the same emission
593 sources.

594 This case demonstrates that major SSA constituents (Na^+_{aer} , Cl^-_{aer} , and CCHO_{aer}) can mix
595 effectively within the boundary layer, reaching altitudes relevant to cloud formation with
596 concentrations nearly identical to ground level, and that such a mixing state can persist during
597 temporarily decoupled conditions, provided there is no additional aerosol particle source at
598 the ground or aloft.

599 ***Case II: Free troposphere decoupled from the ground***

600 On 27 September 2021, balloon measurements were conducted at a median altitude of
601 1112 m, above both the Zeppelin Observatory and the altitude range of Case I, i.e. in the free
602 troposphere above the boundary layer. A strong increase of the potential temperature
603 between 700 m ($\theta \approx 274$ K) and 900 m ($\theta \approx 280$ K) indicates a pronounced inversion (**Figure 5b**).
604 N_{150} peaked near the ground, remained stable in the lowest 200 m, decreased up to ~ 700 m,
605 and slightly increased toward 1112 m, suggesting sources other than the ground. Specific
606 humidity varied strongly (2.6–4 g kg⁻¹), confirming a decoupled atmospheric layer.

607 During ground sampling, mean conditions were 3 °C, 89 % RH, and 0.7 m s⁻¹ wind from the
608 southwest (**Table S5**). At balloon altitude, air was colder (–1.9 °C), slightly drier (87 % RH), and
609 much windier (5.5 m s⁻¹), primarily from the south and southwest (**Table S4**). IWV increased
610 from 13 to ~ 15 kg m⁻² during sampling (**Figure S5b**). A dense warm-front cloud layer (2–8 km)
611 with mainly cloud ice (IWP up to 1.4 kg m⁻²) was present (**Figure S5b**). Precipitation reached
612 the balloon as snowfall only in the last 15–30 min of sampling.

613 On this date, we observed a strong vertical gradient in both Na^+_{aer} and CCHO_{aer} concentrations
614 (**Figure 5b**), starting from the winch (Na^+_{aer} : 1840 ng m⁻³, CCHO_{aer} : 199 ng m⁻³), decreasing at
615 the Zeppelin Observatory (Na^+_{aer} : 850 ng m⁻³), and dropping sharply at the balloon's altitude
616 (Na^+_{aer} : 23 ng m⁻³, CCHO_{aer} : 8.6 ng m⁻³). Similar declines occurred for $\text{SO}^{2-}_{4\text{aer}}$ (580; 220;
617 76 ng m⁻³), Cl^-_{aer} (4230; 1500; 60 ng m⁻³), and $\text{Ca}^{2+}_{\text{aer}}$ (165; 32; 28 ng m⁻³). This pronounced
618 decrease with altitude indicates separation between ground-level and elevated air masses,
619 making fresh local SSA from Kongsfjorden or the west coast of Svalbard an unlikely source for
620 the substances detected at 1112 m.

621 This assumption is supported by back-trajectory analysis (**Figure 6b**): air masses at 50 m and
622 474 m arrival height originated from Arctic pack ice and crossed the ice-free Fram Strait,
623 whereas the 1112 m air mass followed a different path over the Barents Sea near Franz Josef
624 Land. After contact with the marine boundary layer and possibly the sea surface about 48 h
625 before sampling, it remained mainly between 1000 and 1800 m. This indicates that the SSA
626 observed at 1112 m in Ny-Ålesund likely originated from this distant source region.

627 In summary, Case II demonstrates that major SSA constituents (Na_{aer}^+ , $\text{Ca}_{\text{aer}}^{2+}$, Cl_{aer}^- , $\text{SO}_{4\text{ aer}}^{2-}$
628 and CCHO_{aer}) can be present in the free troposphere and likely originate from a distant source.
629 However, they appear at lower concentrations above the inversion than in the boundary layer
630 below, where concentrations, as in Case I, are more similar to those at the ground.

631 ***Case III: Inside and below a drizzling cloud***

632 On 03 October 2021, the ground temperature was 3°C with a high relative humidity of 89%.
633 Winds were light, shifting between east, south, and west at 0.7 m s⁻¹ during sampling. At the
634 balloon's altitude of 666 m, the average temperature was -1.3°C, the relative humidity 96%
635 and the wind speed 6.8 m s⁻¹ from the east and northeast. The day was overcast, with
636 continuous drizzle from a 2 km deep mixed-phase cloud layer with LWP values of up to
637 300 g m⁻² and IWV of around 13 to 14 kg m⁻². The balloon's altitude was close to the melting
638 layer.

639 During the balloon's ascent and descent to 666 m, a positive gradient in potential temperature
640 (272 K at the ground vs. 278 K at the balloon, **Figure 5c**) indicated a stably stratified boundary
641 layer. Specific humidity was uniform (3.2–3.8 g kg⁻¹), while N_{150} was lower than in Case I (3–10
642 cm⁻³) with higher relative variability, likely influenced by low counting statistics at these low
643 concentrations. Overall, mixing conditions in Case III were similar to Case I, but sampling
644 occurred partly within or below a drizzling low-level cloud.

645 Back-trajectory analysis (**Figure 6, Case III**) showed that air masses at the altitudes of ground,
646 balloon, and Zeppelin Observatory followed the same 48-h path from the ice-free ocean south
647 of Svalbard. Vertical trajectory heights indicate shared transport history and influence by the
648 same emission sources, consistent with Case I.

649 In line with the lower aerosol number concentrations, offline measurements of chemical
650 constituents were also generally lower than in the previous cases. Furthermore, major
651 inorganic ions (**Figure 5c**) were generally similar at the ground and balloon (Cl_{aer}^- : 289 &

652 252 ng m⁻³; SO₄²⁻_{aer}: 66 & 59 ng m⁻³; K⁺_{aer}: 23 & 20 ng m⁻³), with Na⁺_{aer} (53 & 35 ng m⁻³)
653 somewhat higher at the ground. At the Zeppelin Observatory, only Na⁺_{aer} exceeded the
654 detection limit, with a concentration of 38 ng m⁻³, very similar to the value observed at the
655 balloon. This consistency indicates a rather mixed boundary layer. Creamean et al. (2021)
656 analyzed three years of Arctic aerosol vertical distributions using a tethered balloon in Alaska
657 and found that, when a uniform aerosol distribution below clouds was observed, it primarily
658 occurred in autumn, aligning well with Case III.

659 Interestingly, despite the same levels of major inorganic ions, some chemical constituents
660 exhibited increased concentrations at higher altitudes. These included major
661 monosaccharides bound within CCHO (ground & balloon: Glc_{CCHO,aer}: 12.6 & 34 ng m⁻³;
662 Xyl_{CCHO,aer}: 0.57 & 4.4 ng m⁻³; Ara_{CCHO,aer}: below detection limit & 0.97 ng m⁻³), as well as
663 oxalate_{aer} (5.5 & 24 ng m⁻³), Ca²⁺_{aer} (47 & 187 ng m⁻³), and Mg²⁺_{aer} (0.97 & 2.6 ng m⁻³). These
664 elevated concentrations cannot be explained by direct local sea spray emissions or remote
665 source contributions alone, suggesting the involvement of cloud-related enrichment and
666 transformation processes.

667 Soluble Ca²⁺_{aer} and Mg²⁺_{aer} possibly derived from preexisting organic structures in SSA,
668 becoming soluble and detectable after chemical aging. OM-bound Ca²⁺, as already found in
669 Antarctic SSA (Su et al., 2023), may originate from SML-derived polysaccharide gels such as
670 TEPs, and airborne algal cells or fragments, which can release Ca²⁺ and Mg²⁺ through gel
671 dispersion or cell dissolution under the acidic conditions of chemically aged SSA aerosol
672 particles (Aller et al., 2017; Angle et al., 2021; Orellana and Leck, 2015; van Pinxteren et al.,
673 2022; Trainic et al., 2018; Zhu et al., 2014). Since these particles were sampled in cloud water,
674 which contains abundant TEP (van Pinxteren et al., 2022), this mechanism may also explain
675 the elevated CCHO concentrations. Ca²⁺_{aer} can form complexes with oxalate_{aer} (Furukawa and
676 Takahashi, 2011), and oxalic acid increases hygroscopicity, potentially accounting for the high
677 values observed at the balloon in Case III. In addition, secondary in-situ atmospheric or
678 microbial origins, particularly in the aqueous phase, may contribute to CCHO_{aer} and oxalate_{aer}
679 and is discussed in the following section.

680 In summary, Case III demonstrates that certain SSA constituents can vary with altitude due to
681 atmospheric processing following primary emissions and vertical transport.

682 Together, the three cases demonstrate that meteorological conditions can lead to similar,
683 lower, or higher concentrations of the investigated chemical constituents across different
684 altitudes. Porter et al. (2022) observed similar patterns for ice-nucleating particles at the
685 North Pole. They combined their measurements with trajectory analyses and heat sensitivity
686 tests to conclude on aerosol sources. While this effect-based approach gives insights into
687 particle properties, direct chemical analyses, as performed in this study, can further enhance
688 certainty about particle origin and composition relevant for cloud formation.

689 **3.3 Factors affecting SSA constituents beyond local sea-air transfer**

690 *Long-range transport and size-dependent deposition*

691 SSA particles originate from both local and remote marine regions. However, our sampling
692 methods make it challenging to determine the relative contribution of long-range transported
693 SSA constituents, particularly when a local marine source, such as the Kongsfjorden is adjacent
694 to the sampling site and may dominate other marine emissions.

695 As demonstrated in Case II, long-range transport of SSA can become dominant when air
696 masses at elevated altitudes are decoupled from those at the ground. In this case, vertical and
697 horizontal trajectory analysis suggests that the measured SSA constituents may have been
698 emitted and incorporated into the atmosphere approximately 48 hours earlier over the
699 Barents Sea, near Franz Josef Land. Typical removal processes of supermicron particles, such
700 as dry and wet deposition or cloud droplet activation, likely reduced the atmospheric
701 concentrations of major inorganic ions and CCHO_{aer} by one to two orders of magnitude before
702 the arrival of the air masses in Ny-Ålesund (**Figure 5b**).

703 In several balloon-borne TSP filter samples, an elevated CCHO_{aer}/Na⁺_{aer} ratio was observed,
704 most notably on 24 Sep 2021; 03 Oct 2021 (Case III) and 03 Apr 2022 (see **Figure 2d**). These
705 values far exceeded both ground-based aerosol measurements from this study and previously
706 reported values (Zeppenfeld et al., 2021, 2023), particularly for supermicron SSA particles that
707 dominate the TSP mass. A slight increase of this ratio may be explained by a longer
708 atmospheric residence time of these particles. This leads to a relative reduction of
709 supermicron aerosol particles, typically dominated by sea salt (O'Dowd and de Leeuw, 2007),
710 through deposition (Croft et al., 2009; Hoppel et al., 2002). In contrast, submicron aerosol
711 particles, which are rich in surface-active CCHO, remain. This process could lead to a shift of
712 the CCHO_{aer}/Na⁺_{aer} ratios more characteristic of submicron than supermicron particles in the
713 TSP samples of this study, as seen in Case II.

714 However, for the three cases with the most pronounced increases in CCHO_{aer}/Na⁺_{aer} ratios in
715 TSP at higher altitudes (24 Sep 2021; 03 Oct 2021; 03 Apr 2022), absolute CCHO_{aer}
716 concentrations were also elevated (compare **Figures 2b and 2d**). Such increases in absolute
717 concentrations cannot be explained by the selective removal of supermicron particles as
718 hypothesized above. This raises the question of whether the observed CCHO_{aer} concentrations

719 could result from the long-range transport of SSA compounds from a distant marine source
720 with significantly higher CCHO levels than the local Kongsfjorden.

721 Model simulations using FESOM2.1-REcoM3 (Gürses et al., 2023) (**Figure S6**) and field data
722 (Assmy et al., 2023; Feltracco et al., 2021; Grosse et al., 2021; Wietz et al., 2024) confirm that
723 the eastern Fram Strait as well as coastal Svalbard waters are productive and polysaccharide-
724 rich regions. While the FESOM2.1-REcoM3 model does not resolve the SML separately,
725 previous studies have shown significant CCHO enrichment in this layer (Compiano et al., 1993;
726 Engel and Galgani, 2016; Gao et al., 2012; Zäncker et al., 2021), particularly in the productive
727 marginal ice zone (Zeppenfeld et al., 2023). However, in cases of high CCHO_{aer} at higher
728 altitudes in this study, air mass trajectories did not pass over any of these productive marine
729 regions within 48 hours before reaching Svalbard (**Figure S7**). These findings suggest that long-
730 range transport of SSA from more productive remote marine sources is unlikely to explain the
731 elevated CCHO_{aer} concentrations at elevated altitudes within the lower troposphere in Ny-
732 Ålesund, further supporting a predominantly local source or atmospheric in-situ formation.

733 In summary, while long-range transport of SSA constituents at elevated altitudes appears
734 relevant in cases of decoupled atmospheric layers such as in Case II, it may not explain the
735 significantly higher CCHO_{aer} concentrations at high altitudes compared to ground levels.
736 Instead, in-situ formation of CCHO_{aer} could be a more plausible explanation for these
737 observations.

738

739 ***Atmospheric in-situ formation of marine CCHO_{aer}***

740 Bacteria can be transported into and persist in the Arctic atmosphere (Jensen et al., 2022;
741 Šantl-Temkiv et al., 2018), with sources including terrestrial environments and surface
742 seawater, particularly the SML (Aller et al., 2005). Our complementary microbiological
743 sampling during our campaign supported such dynamics by detecting diverse marine bacteria
744 in aerosol particles (Wietz et al., 2025). Some aerosolized taxa, for instance *Polaribacter*,
745 encode multiple genes for CCHO metabolism (Avci et al., 2020) and consistently occur in both
746 Kongsfjorden seawater and atmosphere during the spring bloom (Feltracco et al., 2021). These
747 observations might underpin microbial CCHO transformations in the atmosphere, for instance
748 the production of polysaccharide-based gels as protection against temperature fluctuations,
749 salinity changes, and desiccation (Aller et al., 2005; Ramasamy et al., 2023; Šantl-Temkiv et al.,

750 2022). Under highly humid conditions, especially in the presence of liquid water (such as in
751 Case III), airborne bacteria can become metabolically active (Ervens and Amato, 2020;
752 Haddrell and Thomas, 2017). Atmospheric OM formation, including CCHO, through microbial
753 activity has been documented for cloud water and aerosol particles (Bianco et al., 2019; Klein
754 et al., 2016; Matulová et al., 2014). Although substantial uncertainties remain, Zeppenfeld et
755 al. (2021) estimated, depending on parameter choice, residence times between 20 minutes
756 and several hundred hours during which measurable microbial transformation of
757 carbohydrates in the atmosphere may occur. Consequently, metabolically active bacteria in
758 the atmosphere could explain the increased CCHO_{aer} concentrations observed within or near
759 drizzling clouds in Case III of this study.

760 ***CCHO_{aer} versus oxalate_{aer}: Co-production or atmospheric processing?***

761 Since both combined glucose and combined xylose were consistently detected in CCHO_{aer} of
762 nearly all aerosol samples, we examined their correlation with other atmospheric chemical
763 parameters. We observed a strong correlation between atmospheric xylose in CCHO_{aer} and
764 oxalate_{aer} with an $R=0.78$ ($p<0.001$) across all sampling locations and heights (**Figure 7**).
765 Oxalate, the ionic form of oxalic acid, is the most abundant dicarboxylic acid in aerosol
766 particles (Kerminen et al., 1999; Rinaldi et al., 2011), with atmospheric concentrations in this
767 study between <1 and 67 ng m^{-3} . The strong correlation raised the question of whether oxalic
768 acid could be chemically linked to combined carbohydrates in aerosol particles.

769 Oxalate_{aer} is known to originate from several primary sources and secondary formation
770 pathways in both terrestrial and anthropogenic environments (Kawamura and Bikkina, 2016;
771 Yang et al., 2022). In remote marine environments, the atmospheric formation of oxalic acid
772 was proposed by Warneck (2003) through the aqueous-phase oxidation of glyoxal and
773 glycolaldehyde, a process also investigated by field measurements inside and above marine
774 clouds (Crahan et al., 2004; Sorooshian et al., 2007) and modeling (Herrmann et al., 2005;
775 Tilgner and Herrmann, 2010). The possible aqueous-phase formation was supported by Case
776 III of this study, where higher oxalate_{aer} concentrations were observed within and in vicinity of
777 clouds compared to ground level. In contrast, in the drier conditions of Cases I and II, oxalate_{aer}
778 levels remained vertically uniform. Additionally, since overall oxalate_{aer} levels at the Old Pier
779 ($1.1\text{--}10.1 \text{ ng m}^{-3}$; $\text{mean}=4.3\pm 3.5 \text{ ng m}^{-3}$) were relatively low compared to the more inland

780 Winch ($<1\text{--}58\text{ ng m}^{-3}$; $\text{mean}=19.8\pm 16.2\text{ ng m}^{-3}$) and elevated altitudes samples ($4.6\text{--}67\text{ ng m}^{-3}$;
781 $\text{mean}=29.6\pm 17.8\text{ ng m}^{-3}$), direct primary oceanic emission was likely not its dominant source.

782

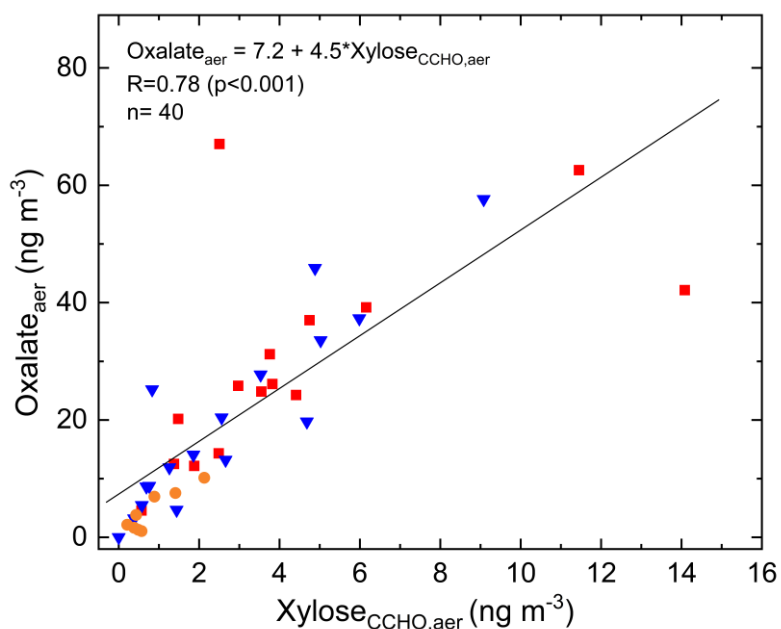


Figure 7. Atmospheric oxalate as a function of xylose in CCHO_{aer} ($R=0.78$; $p<0.001$) measured in TSP from the Old Pier (orange circles), the winch site (blue triangles) and at elevated altitudes (red squares).

791 But what are the precursors of glyoxal and glycolaldehyde, the precursors of oxalic acid? While
792 Warneck (2003) suggested that the anthropogenic volatile organic compounds acetylene and
793 ethene can be transformed to atmospheric glyoxal, other studies suggest the photochemical
794 degradation of marine OM (McNeill, 2015; Sinreich et al., 2010; Turekian et al., 2003; Zhou et
795 al., 2014), with oligo- and polysaccharides representing a known subclass. Although not
796 explicitly measured in this study, previous findings have shown that both CCHO_{aer} (Leck et al.,
797 2013; Zeppenfeld et al., 2021, 2023) and oxalate_{aer} (Guo et al., 2016; Rinaldi et al., 2011;
798 Turekian et al., 2003) are present across both the accumulation and coarse size modes.
799 However, no consistently dominant size mode has been identified, which may support a
800 common mechanism of formation or similar atmospheric processing pathways.

801 Here, based on known chemical reactions, we propose possible atmospheric pathways linking
802 xylose-containing oligo- and polysaccharides as the precursors to oxalate as the final product
803 (**Figure 8**). The initial depolymerization of CCHO presumably occurs either via enzymatic
804 degradation, e.g. by glycoside hydrolases, or acid hydrolysis (Panagiotopoulos and Sempéré,

2005), both of which are plausible in the atmospheric context. Active microbial enzymes have been detected in SSA, often exhibiting activities 1–2 orders of magnitude higher than in bulk seawater (Malfatti et al., 2019). Additionally, SSA particles are known for reaching very low pH levels within minutes after their emissions due to the uptake and reactions with acidic gases, as well as water loss (Angle et al., 2022, 2021). Furthermore, although not explicitly investigated in an atmospheric context, Zhu et al. (2023) observed rapid depolymerization of xylose-containing oligosaccharides into the monosaccharide xylose within minutes in a UV/H₂O₂ system, which generates hydroxyl radicals.

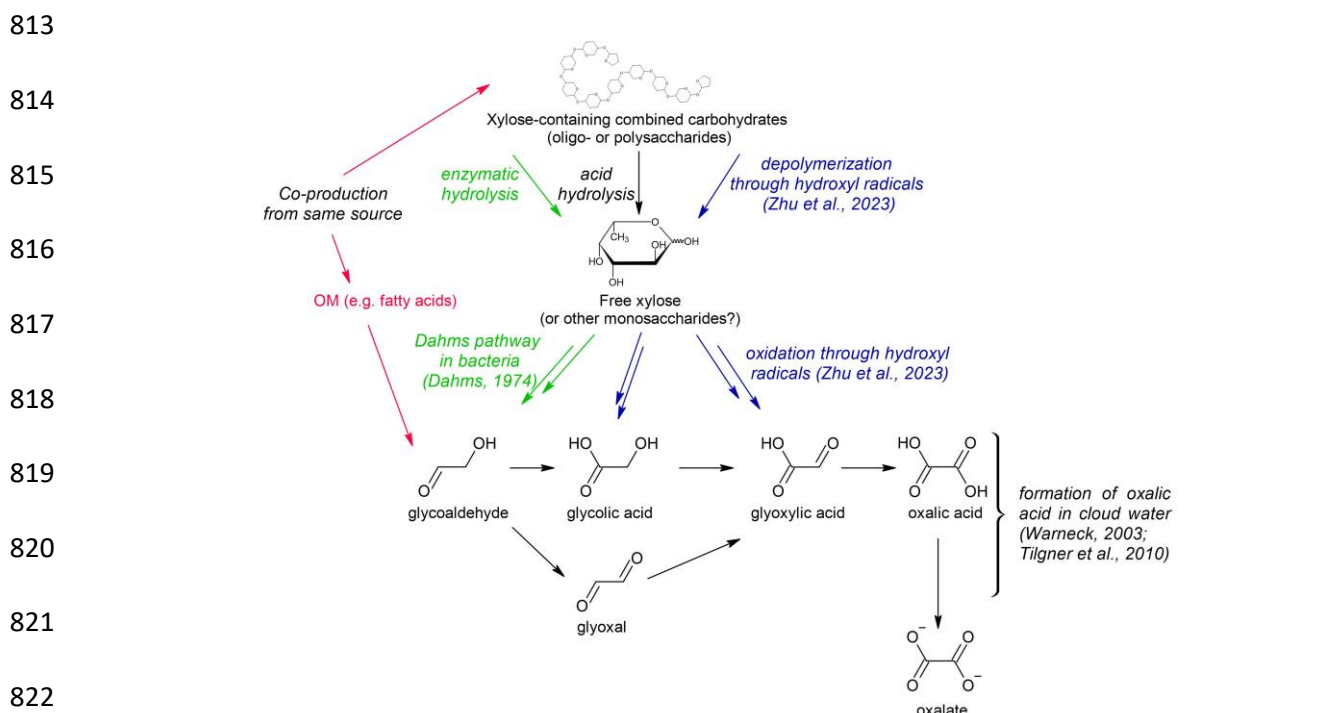


Figure 8. Possible pathways for the formation of atmospheric oxalate from xylose in combined carbohydrates in marine aerosol particles.

With one exception, free xylose was never detected in any aerosol sample of this study. This suggests two possible explanations. First, xylose may have remained bound within the CCHO_{aer} fraction and was not released into its free form. In this case, it would indicate co-emission without a chemical pathway leading to oxalate. Second, free xylose may have been rapidly processed in the atmosphere via reactions described below.

Two potential pathways may link monomeric xylose to precursors of Warneck's oxalate formation: (1) a follow-up reaction with hydroxyl radicals, where the pyranose ring of xylose is cleaved after the more susceptible glycosidic bonds have been readily broken. Zhu et al.

831 (2023) observed glycolic acid and glyoxylic acid among other products following the UV/H₂O₂
832 treatment of xylooligosaccharides. (2) Bacterial metabolism via the Dahms pathway
833 converting free xylose into pyruvate and glycolaldehyde (Dahms, 1974). However, only few
834 bacteria encode this pathway; and it is highly questionable whether these occur in sufficient
835 atmospheric concentrations for a measurable effect.

836 One indication that direct formation from xylose-containing oligo- and polysaccharides cannot
837 be the sole source of atmospheric oxalate in the marine environment is the discrepancy in
838 concentrations: atmospheric oxalate levels were seven times higher than those of combined
839 xylose. This confirms the involvement of additional precursors or a co-production/co-emission
840 of combined xylose with gaseous precursors, such as isoprene (Carlton et al., 2009; Kawamura
841 and Bikina, 2016), or other primary marine organic matter, such as phytoplankton-derived
842 fatty acids (Kawamura et al., 1996a, b) undergoing photo-oxidation. Further targeted
843 laboratory and modeling studies are needed for clarity.

844 **4. Summary and Atmospheric Implications**

845 In autumn 2021 and spring 2022, we performed balloon-borne measurements of major SSA
846 constituents at Ny-Ålesund (Svalbard). Our evidence demonstrated that both sodium and
847 marine CCHO reach elevated altitudes within the boundary layer, and even the free
848 troposphere as part of aerosol particles. The relationship between ground-level and high-
849 altitude measurements was strongly influenced by meteorological conditions and the mixing
850 state of the lower atmosphere, as discussed in three representative cases. Long-range
851 transport of Na^+_{aer} and CCHO_{aer} from remote marine sources is presumably relevant for high-
852 altitude measurements, especially when the upper air masses were decoupled from the
853 ground. However, in cases of a well-mixed lower atmosphere, the local marine source (here,
854 the Kongsfjorden) was the dominant contributor for atmospheric Na^+_{aer} and CCHO_{aer} . Under
855 very humid conditions particularly in the presence of liquid precipitating clouds, in-situ
856 formation of CCHO_{aer} was observed, possibly linked to microbial metabolism. To establish
857 more generalizable patterns, we recommend further field studies using airborne platforms.

858 The significant correlation between combined xylose within CCHO_{aer} , and $\text{oxalate}_{\text{aer}}$ suggests
859 underlying pathways for oxalic acid formation from combined xylose and other
860 monosaccharide units within CCHO_{aer} ; alternatively, a co-production of xylose-containing
861 oligo- and polysaccharides alongside oxalate precursors.

862 Cloud condensation nuclei and ice-nucleating particles are key drivers in cloud formation,
863 influencing radiative and precipitation properties and, consequently, climate processes.
864 Considerable uncertainties remain regarding the origin and chemical composition of these
865 particles, particularly in remote Arctic regions, which affects the accuracy of climate models.
866 Since marine polysaccharides have been identified as relevant ice-nucleating molecules in the
867 remote marine atmosphere (Hartmann et al., 2025), our findings have implications for cloud
868 microphysics, especially given that these carbohydrates are transported to altitudes relevant
869 for cloud formation. Furthermore, atmospheric processing, as observed here, may alter the
870 ice-nucleating properties of these macromolecules, potentially creating new ice-nucleating
871 particles in-situ or deactivating existing ones.

872 As the Arctic continues to change, expanding ice-free ocean areas will serve as emission
873 sources for SSA particles, influencing cloud properties, and finally the radiative budget.

874 Consequently, our findings contribute to an improved understanding of the complex interplay
875 of environmental processes resulting in Arctic amplification (Wendisch et al., 2017, 2023).

876 **Author contributions**

877 SZ wrote the manuscript with input from all co-authors. SZ, JS, CP, HS, BW, MW, and MvP
878 collected field samples in Ny-Ålesund. HS and BW served as principal investigators for balloon
879 operations during the field campaign. SZ conducted the laboratory carbohydrate analyses and
880 data processing. MZ and AB carried out the FESOM2.1-REcoM3 simulations. KE assessed cloud
881 conditions for the case studies using remote sensing data. All co-authors reviewed and
882 commented on the manuscript.

883

884 **Acknowledgments**

885 We would like to express our gratitude to Kings Bay and the AWIPEV staff, with special thanks
886 to the station leader Grégory Tran, for their invaluable support to make this field study
887 possible. We furthermore thank the AWIPEV station's scientific staff in ensuring the
888 availability of high-quality meteorological data. In this context, we like to give special thanks
889 to Fieke Rader and Marion Maturilli. The cloud observations were taken within the project
890 AWIPEV_0016.

891 We also thank the scientific team at the Zeppelin Observatory from NILU and NPI, with special
892 appreciation to Wenche Aas, for their dedicated work in monitoring aerosol data.

893 Furthermore, we acknowledge the entire BELUGA team for their contributions during both
894 the autumn 2021 and spring 2022 campaigns, with special thanks to Thomas Conrath. We also
895 thank Michel Michalkow for preprocessing the CAMP and standard meteorological data
896 collected at BELUGA as part of his Master's thesis. We are grateful to René Rabe for preparing
897 the campaign equipment and to Leon Schmidt for conducting the chemical analysis of
898 inorganic ions.

899 For the FESOM2.1-REcoM3 simulation for this research, the authors gratefully acknowledge
900 the computing time granted by the Resource Allocation Board and provided on the
901 supercomputer Lise and Emmy at NHR@ZIB and NHR@Göttingen as part of the NHR

902 infrastructure. The calculations for this research were conducted with computing resources
903 under the project hbk00084.

904 This research has been supported by the Deutsche Forschungsgemeinschaft (DFG, German
905 Research Foundation, project no. 268020496-TRR 172) within the Transregional Collaborative
906 Research Center “ArctiC Amplification: Climate Relevant Atmospheric and SurfaCe Processes,
907 and Feedback Mechanisms (AC)3” in subprojects A02, B04, C03 and E02. MW was supported
908 by the DFG Priority Program SPP 1158 “Antarctic Research with comparative investigations in
909 Arctic ice areas” (grant 522416631). We thank Johannes Röttenbacher for his constructive
910 feedback on the manuscript.

911

912 **Competing interests**

913 All authors declare no financial or non-financial competing interests. Some authors are
914 members of the editorial board of ACP.

915

916 **Data availability**

917 Chemical data from offline TSP filters are publicly available in PANGAEA for seawater
918 (Zeppenfeld and Schmidt, 2025) and aerosol particles (Zeppenfeld et al., 2025). The
919 microwave radiometer LWP and IWV data are available in PANGAEA (Ebell and Ritter, 2022).
920 The Cloudnet classification and ice water content products (Ebell et al., 2025) can be
921 downloaded via the ACTRIS Cloudnet data portal (<https://cloudnet.fmi.fi>).

922 References

- 923 Aas, W., Berglen, T. F., Eckhardt, S., Fiebig, M., Solberg, S., and Yttri, K. E.: Monitoring of long-range transported air pollutants
924 in Norway. Annual Report 2021., NILU, 2022.
- 925 Aas, W., Eckhardt, S., Solberg, S., and Yttri, K. E.: Monitoring of long-range transported air pollutants in Norway. Annual Report
926 2022., NILU, 2023.
- 927 Akansu, E. F., Dahlke, S., Siebert, H., and Wendisch, M.: Evaluation of methods to determine the surface mixing layer height
928 of the atmospheric boundary layer in the central Arctic during polar night and transition to polar day in cloudless and cloudy
929 conditions, *Atmospheric Chemistry and Physics*, 23, 15473–15489, <https://doi.org/10.5194/acp-23-15473-2023>, 2023.
- 930 Aller, J. Y., Kuznetsova, M. R., Jahns, C. J., and Kemp, P. F.: The sea surface microlayer as a source of viral and bacterial
931 enrichment in marine aerosols, *Journal of Aerosol Science*, 36, 801–812, <https://doi.org/10.1016/j.jaerosci.2004.10.012>,
932 2005.
- 933 Aller, J. Y., Radway, J. C., Kilhau, W. P., Bothe, D. W., Wilson, T. W., Vaillancourt, R. D., Quinn, P. K., Coffman, D. J., Murray,
934 B. J., and Knopf, D. A.: Size-resolved characterization of the polysaccharidic and proteinaceous components of sea spray
935 aerosol, *Atmospheric Environment*, 154, 331–347, <https://doi.org/10.1016/j.atmosenv.2017.01.053>, 2017.
- 936 Alpert, P. A., Kilhau, W. P., O'Brien, R. E., Moffet, R. C., Gilles, M. K., Wang, B., Laskin, A., Aller, J. Y., and Knopf, D. A.: Ice-
937 nucleating agents in sea spray aerosol identified and quantified with a holistic multimodal freezing model, *Science Advances*,
938 8, eabq6842, <https://doi.org/10.1126/sciadv.abq6842>, 2022.
- 939 Aluwihare, L. I., Repeta, D. J., and Chen, R. F.: A major biopolymeric component to dissolved organic carbon in surface sea
940 water, *Nature*, 387, 166–169, <https://doi.org/10.1038/387166a0>, 1997.
- 941 Amore, A., Giardi, F., Becagli, S., Caiazza, L., Mazzola, M., Severi, M., and Traversi, R.: Source apportionment of sulphate in
942 the High Arctic by a 10 yr-long record from Gruevbadet Observatory (Ny-Ålesund, Svalbard Islands), *Atmospheric
943 Environment*, 270, 118890, <https://doi.org/10.1016/j.atmosenv.2021.118890>, 2022.
- 944 Angle, K., Grassian, V. H., and Ault, A. P.: The rapid acidification of sea spray aerosols, *Physics today*, 75, 58–59,
945 <https://doi.org/10.1063/PT.3.4926>, 2022.
- 946 Angle, K. J., Crocker, D. R., Simpson, R. M. C., Mayer, K. J., Garofalo, L. A., Moore, A. N., Garcia, S. L. M., Or, V. W., Srinivasan,
947 S., Farhan, M., Sauer, J. S., Lee, C., Pothier, M. A., Farmer, D. K., Martz, T. R., Bertram, T. H., Cappa, C. D., Prather, K. A., and
948 Grassian, V. H.: Acidity across the interface from the ocean surface to sea spray aerosol, *PNAS*, 118, 1–6,
949 <https://doi.org/10.1073/pnas.2018397118>, 2021.
- 950 Arnosti, C., Wietz, M., Brinkhoff, T., Hehemann, J.-H., Probandt, D., Zeugner, L., and Amann, R.: The Biogeochemistry of
951 Marine Polysaccharides: Sources, Inventories, and Bacterial Drivers of the Carbohydrate Cycle, *Ann Rev Mar Sci*, 13, 81–108,
952 <https://doi.org/10.1146/annurev-marine-032020-012810>, 2021.
- 953 Assmy, P., Cecilie Kvernvik, A., Hop, H., Hoppe, C. J. M., Chierici, M., David T., D., Duarte, P., Fransson, A., García, L. M., Patuła,
954 W., Kwaśniewski, S., Maturilli, M., Pavlova, O., Tatarek, A., Wiktor, J. M., Wold, A., Wolf, K. K. E., and Bailey, A.: Seasonal
955 plankton dynamics in Kongsfjorden during two years of contrasting environmental conditions, *Progress in Oceanography*,
956 213, 102996, <https://doi.org/10.1016/j.pocean.2023.102996>, 2023.
- 957 Avci, B., Krüger, K., Fuchs, B. M., Teeling, H., and Amann, R. I.: Polysaccharide niche partitioning of distinct *Polaribacter* clades
958 during North Sea spring algal blooms, *ISME J*, 14, 1369–1383, <https://doi.org/10.1038/s41396-020-0601-y>, 2020.
- 959 Barthelmeß, T., Cristi, A., Deppeler, S., Safi, K., Sellegrì, K., Law, C. S., and Engel, A.: Pronounced Diel Cycling of Dissolved
960 Carbohydrates and Amino Acids in the Surface Ocean and across Diverse Regimes, *Environ. Sci. Technol.*, 59, 419–429,
961 <https://doi.org/10.1021/acs.est.4c00491>, 2025.
- 962 Becker, S., Tebben, J., Coffinet, S., Wiltshire, K., Iversen, M. H., Harder, T., Hinrichs, K.-U., and Hehemann, J.-H.: Laminarin is
963 a major molecule in the marine carbon cycle, *PNAS*, 117, 6599–6607, <https://doi.org/10.1073/pnas.1917001117>, 2020.
- 964 Bianco, A., Deguillaume, L., Chaumerliac, N., Vařtilingom, M., Wang, M., Delort, A.-M., and Bridoux, M. C.: Effect of
965 endogenous microbiota on the molecular composition of cloud water: a study by Fourier-transform ion cyclotron resonance
966 mass spectrometry (FT-ICR MS), *Sci Rep*, 9, 1–12, <https://doi.org/10.1038/s41598-019-44149-8>, 2019.
- 967 Bischof, K., Convey, P., Duarte, P., Gattuso, J.-P., Granberg, M., Hop, H., Hoppe, C., Jiménez, C., Lisitsyn, L., Martínez, B.,
968 Roleda, M. Y., Thor, P., Wiktor, J. M., and Gabrielsen, G. W.: Kongsfjorden as Harbinger of the Future Arctic: Knowns,
969 Unknowns and Research Priorities, in: *The Ecosystem of Kongsfjorden, Svalbard*, edited by: Hop, H. and Wiencke, C., Springer
970 International Publishing, Cham, 537–562, https://doi.org/10.1007/978-3-319-46425-1_14, 2019.
- 971 Bivand, R., Pebesma, E., and Gomez-Rubio, V.: *Applied spatial data analysis with R*, Springer, 2013.
- 972 Bivand, R., Keitt, T., and Rowlingson, B.: *rgdal: Bindings for the “Geospatial” Data Abstraction Library*, R package version 1.5-
973 32, 2022.

974 Borch, N. H. and Kirchman, D. L.: Concentration and composition of dissolved combined neutral sugars (polysaccharides) in
975 seawater determined by HPLC-PAD, *Marine Chemistry*, 57, 85–95, [https://doi.org/10.1016/S0304-4203\(97\)00002-9](https://doi.org/10.1016/S0304-4203(97)00002-9), 1997.

976 Brownrigg, M. R.: Package ‘mapdata, R package version 2.3.1, 2013.

977 Brownrigg, M. R.: maps: Draw Geographical Maps, R package version 3.4.2, 2023.

978 Browse, J., Carslaw, K. S., Mann, G. W., Birch, C. E., Arnold, S. R., and Leck, C.: The complex response of Arctic aerosol to sea-
979 ice retreat, *Atmospheric Chemistry and Physics*, 14, 7543–7557, <https://doi.org/10.5194/acp-14-7543-2014>, 2014.

980 Burns, W. G., Marchetti, A., and Ziervogel, K.: Enhanced formation of transparent exopolymer particles (TEP) under
981 turbulence during phytoplankton growth, *J Plankton Res*, 41, 349–361, <https://doi.org/10.1093/plankt/fbz018>, 2019.

982 Burrows, S. M., Ogunro, O., Frossard, A., Russell, L. M., Rasch, P. J., and Elliott, S.: A Physically Based Framework for Modelling
983 the Organic Fractionation of Sea Spray Aerosol from Bubble Film Langmuir Equilibria, *Atmospheric Chemistry and Physics*,
984 14(24):13601–13629, <https://doi.org/10.5194/acp-14-13601-2014>, 2014.

985 Cai, Q., Wang, J., Beletsky, D., Overland, J., Ikeda, M., and Wan, L.: Accelerated decline of summer Arctic sea ice during 1850–
986 2017 and the amplified Arctic warming during the recent decades, *Environ. Res. Lett.*, 16, 034015,
987 <https://doi.org/10.1088/1748-9326/abdb5f>, 2021.

988 Carlton, A. G., Wiedinmyer, C., and Kroll, J. H.: A review of Secondary Organic Aerosol (SOA) formation from isoprene,
989 *Atmospheric Chemistry and Physics*, 9, 4987–5005, <https://doi.org/10.5194/acp-9-4987-2009>, 2009.

990 Carslaw, D. C. and Ropkins, K.: openair --- An R package for air quality data analysis, *Environmental Modelling & Software*,
991 27–28, 52–61, 2012.

992 Chang, L., Song, S., Feng, G., Zhang, Y., and Gao, G.: Assessment of the Uncertainties in Arctic Low-Level Temperature
993 Inversion Characteristics in Radio Occultation Observations, *IEEE Transactions on Geoscience and Remote Sensing*, 55, 1793–
994 1803, <https://doi.org/10.1109/TGRS.2016.2633461>, 2017.

995 Chi, J. W., Li, W. J., Zhang, D. Z., Zhang, J. C., Lin, Y. T., Shen, X. J., Sun, J. Y., Chen, J. M., Zhang, X. Y., Zhang, Y. M., and Wang,
996 W. X.: Sea salt aerosols as a reactive surface for inorganic and organic acidic gases in the Arctic troposphere, *Atmospheric
997 Chemistry and Physics*, 15, 11341–11353, <https://doi.org/10.5194/acp-15-11341-2015>, 2015.

998 Compiano, A.-M., Romano, J.-C., Garabetian, F., Laborde, P., and de la Giraudière, I.: Monosaccharide composition of
999 particulate hydrolysable sugar fraction in surface microlayers from brackish and marine waters, *Marine Chemistry*, 42, 237–
1000 251, [https://doi.org/10.1016/0304-4203\(93\)90015-G](https://doi.org/10.1016/0304-4203(93)90015-G), 1993.

1001 Crahan, K. K., Hegg, D., Covert, D. S., and Jonsson, H.: An exploration of aqueous oxalic acid production in the coastal marine
1002 atmosphere, *Atmospheric Environment*, 38, 3757–3764, <https://doi.org/10.1016/j.atmosenv.2004.04.009>, 2004.

1003 Creamean, J. M., de Boer, G., Telg, H., Mei, F., Dexheimer, D., Shupe, M. D., Solomon, A., and McComiskey, A.: Assessing the
1004 vertical structure of Arctic aerosols using balloon-borne measurements, *Atmospheric Chemistry and Physics*, 21, 1737–1757,
1005 <https://doi.org/10.5194/acp-21-1737-2021>, 2021.

1006 Croft, B., Lohmann, U., Martin, R. V., Stier, P., Wurzler, S., Feichter, J., Posselt, R., and Ferrachat, S.: Aerosol size-dependent
1007 below-cloud scavenging by rain and snow in the ECHAM5-HAM, *Atmospheric Chemistry and Physics*, 9, 4653–4675,
1008 <https://doi.org/10.5194/acp-9-4653-2009>, 2009.

1009 Cunliffe, M. and Wurl, O.: Guide to best practices to study the ocean’s surface., *Marine Biological Association of the United
1010 Kingdom for SCOR*, 2014.

1011 Dahms, A. S.: 3-Deoxy-D-pentulosonic acid aldolase and its role in a new pathway of D-xylose degradation, *Biochemical and
1012 Biophysical Research Communications*, 60, 1433–1439, [https://doi.org/10.1016/0006-291X\(74\)90358-1](https://doi.org/10.1016/0006-291X(74)90358-1), 1974.

1013 Dekhtyareva, A., Holmén, K., Maturilli, M., Hermansen, O., and Graversen, R.: Effect of seasonal mesoscale and microscale
1014 meteorological conditions in Ny-Ålesund on results of monitoring of long-range transported pollution, *Polar Research*, 2018.

1015 DeMott, P. J., Hill, T. C. J., McCluskey, C. S., Prather, K. A., Collins, D. B., Sullivan, R. C., Ruppel, M. J., Mason, R. H., Irish, V. E.,
1016 Lee, T., Hwang, C. Y., Rhee, T. S., Snider, J. R., McMeeking, G. R., Dhaniyala, S., Lewis, E. R., Wentzell, J. J. B., Abbatt, J., Lee,
1017 C., Sultana, C. M., Ault, A. P., Axson, J. L., Martinez, M. D., Venero, I., Santos-Figueroa, G., Stokes, M. D., Deane, G. B., Mayol-
1018 Bracero, O. L., Grassian, V. H., Bertram, T. H., Bertram, A. K., Moffett, B. F., and Franc, G. D.: Sea spray aerosol as a unique
1019 source of ice nucleating particles, *PNAS*, 113, 5797–5803, <https://doi.org/10.1073/pnas.1514034112>, 2016.

1020 Dusek, U., Frank, G. P., Hildebrandt, L., Curtius, J., Schneider, J., Walter, S., Chand, D., Drewnick, F., Hings, S., Jung, D.,
1021 Borrmann, S., and Andreae, M. O.: Size Matters More Than Chemistry for Cloud-Nucleating Ability of Aerosol Particles,
1022 *Science*, 312, 1375–1378, <https://doi.org/10.1126/science.1125261>, 2006.

1023 Ebell, K. and Ritter, C.: HATPRO microwave radiometer measurements at AWIPEV, Ny-Ålesund (2019-2021), PANGAEA,
1024 <https://doi.org/10.1594/PANGAEA.943004>, 2022.

1025 Ebell, K., Maturilli, M., Ritter, C., and O’Connor, E.: Custom collection of classification, and ice water content data from Ny-
1026 Ålesund between 27 Sep and 12 Nov 2021, ACTRIS Cloud remote sensing data centre unit (CLU),
1027 <https://doi.org/10.60656/5598100185854c01>, 2025.

- 1028 Egerer, U., Ehrlich, A., Gottschalk, M., Griesche, H., Neggers, R. A. J., Siebert, H., and Wendisch, M.: Case study of a humidity
1029 layer above Arctic stratocumulus and potential turbulent coupling with the cloud top, *Atmospheric Chemistry and Physics*,
1030 21, 6347–6364, <https://doi.org/10.5194/acp-21-6347-2021>, 2021.
- 1031 Egerer, U., Siebert, H., Hellmuth, O., and Sørensen, L. L.: The role of a low-level jet for stirring the stable atmospheric surface
1032 layer in the Arctic, *Atmospheric Chemistry and Physics*, 23, 15365–15373, <https://doi.org/10.5194/acp-23-15365-2023>, 2023.
- 1033 Engel, A.: Distribution of transparent exopolymer particles (TEP) in the northeast Atlantic Ocean and their potential
1034 significance for aggregation processes, *Deep Sea Research Part I: Oceanographic Research Papers*, 51, 83–92,
1035 <https://doi.org/10.1016/j.dsr.2003.09.001>, 2004.
- 1036 Engel, A. and Galgani, L.: The organic sea-surface microlayer in the upwelling region off the coast of Peru and potential
1037 implications for air–sea exchange processes, *Biogeosciences (BG)*, 13, 989–1007, <https://doi.org/10.5194/bg-13-989-2016>,
1038 2016.
- 1039 Engel, A. and Händel, N.: A novel protocol for determining the concentration and composition of sugars in particulate and in
1040 high molecular weight dissolved organic matter (HMW-DOM) in seawater, *Marine Chemistry*, 127, 180–191,
1041 <https://doi.org/10.1016/j.marchem.2011.09.004>, 2011.
- 1042 Engel, A., Thoms, S., Riebesell, U., Rochelle-Newall, E., and Zondervan, I.: Polysaccharide aggregation as a potential sink of
1043 marine dissolved organic carbon, *Nature*, 428, 929–932, <https://doi.org/10.1038/nature02453>, 2004.
- 1044 Engel, A., Harlay, J., Piontek, J., and Chou, L.: Contribution of combined carbohydrates to dissolved and particulate organic
1045 carbon after the spring bloom in the northern Bay of Biscay (North-Eastern Atlantic Ocean), *Continental Shelf Research*, 45,
1046 42–53, <https://doi.org/10.1016/j.csr.2012.05.016>, 2012.
- 1047 Ervens, B. and Amato, P.: The global impact of bacterial processes on carbon mass, *Atmospheric Chemistry & Physics*, 20,
1048 1777–1794, <https://doi.org/10.5194/acp-20-1777-2020>, 2020.
- 1049 Esau, I. and Repina, I.: Wind Climate in Kongsfjorden, Svalbard, and Attribution of Leading Wind Driving Mechanisms through
1050 Turbulence-Resolving Simulations, *Advances in Meteorology*, 2012, 568454, <https://doi.org/10.1155/2012/568454>, 2012.
- 1051 Fabiano, M., Povero, P., and Danovaro, R.: Distribution and composition of particulate organic matter in the Ross Sea
1052 (Antarctica), *Polar Biol*, 13, 525–533, <https://doi.org/10.1007/BF00236394>, 1993.
- 1053 Facchini, M. C., Rinaldi, M., Decesari, S., Carbone, C., Finessi, E., Mircea, M., Fuzzi, S., Ceburnis, D., Flanagan, R., Nilsson, E. D.,
1054 Leeuw, G. de, Martino, M., Woeltjen, J., and O’Dowd, C. D.: Primary submicron marine aerosol dominated by insoluble organic
1055 colloids and aggregates, *Geophysical Research Letters*, 35, 1–5, <https://doi.org/10.1029/2008GL034210>, 2008.
- 1056 Farmer, D. K., Cappa, C. D., and Kreidenweis, S. M.: Atmospheric Processes and Their Controlling Influence on Cloud
1057 Condensation Nuclei Activity, *Chem. Rev.*, 115, 4199–4217, <https://doi.org/10.1021/cr5006292>, 2015.
- 1058 Farmer, D. K., Boedicker, E. K., and DeBolt, H. M.: Dry Deposition of Atmospheric Aerosols: Approaches, Observations, and
1059 Mechanisms, *Annual Review of Physical Chemistry*, 72, 375–397, <https://doi.org/10.1146/annurev-physchem-090519-034936>, 2021.
- 1061 Feltracco, M., Barbaro, E., Hoppe, C. J. M., Wolf, K. K. E., Spolaor, A., Layton, R., Keuschnig, C., Barbante, C., Gambaro, A., and
1062 Larose, C.: Airborne bacteria and particulate chemistry capture Phytoplankton bloom dynamics in an Arctic fjord, *Atmospheric
1063 Environment*, 256, 118458, <https://doi.org/10.1016/j.atmosenv.2021.118458>, 2021.
- 1064 Fomba, K. W., Müller, K., van Pinxteren, D., Poulain, L., van Pinxteren, M., and Herrmann, H.: Long-term chemical
1065 characterization of tropical and marine aerosols at the Cape Verde Atmospheric Observatory (CVAO) from 2007 to 2011,
1066 *Atmospheric Chemistry and Physics*, 14, 8883–8904, <https://doi.org/10.5194/acp-14-8883-2014>, 2014.
- 1067 Francis, J. A. and Wu, B.: Why has no new record-minimum Arctic sea-ice extent occurred since September 2012?, *Environ.
1068 Res. Lett.*, 15, 114034, <https://doi.org/10.1088/1748-9326/abc047>, 2020.
- 1069 Freud, E., Krejci, R., Tunved, P., Leaitch, R., Nguyen, Q. T., Massling, A., Skov, H., and Barrie, L.: Pan-Arctic aerosol number size
1070 distributions: seasonality and transport patterns, *Atmospheric Chemistry and Physics*, 17, 8101–8128,
1071 <https://doi.org/10.5194/acp-17-8101-2017>, 2017.
- 1072 Furukawa, T. and Takahashi, Y.: Oxalate metal complexes in aerosol particles: implications for the hygroscopicity of oxalate-
1073 containing particles, *Atmos. Chem. Phys.*, 11, 4289–4301, <https://doi.org/10.5194/acp-11-4289-2011>, 2011.
- 1074 Gantt, B., Meskhidze, N., Facchini, M. C., Rinaldi, M., Ceburnis, D., and O’Dowd, C. D.: Wind speed dependent size-resolved
1075 parameterization for the organic mass fraction of sea spray aerosol, *Atmospheric Chemistry and Physics*, 11, 8777–8790,
1076 <https://doi.org/10.5194/acp-11-8777-2011>, 2011.
- 1077 Gao, Q., Leck, C., Rauschenberg, C., and Matrai, P. A.: On the chemical dynamics of extracellular polysaccharides in the high
1078 Arctic surface microlayer, *Ocean Science*, 8, 401–418, <https://doi.org/10.5194/os-8-401-2012>, 2012.
- 1079 Gierens, R., Kneifel, S., Shupe, M. D., Ebell, K., Maturilli, M., and Löhnert, U.: Low-level mixed-phase clouds in a complex Arctic
1080 environment, *Atmospheric Chemistry and Physics*, 20, 3459–3481, <https://doi.org/10.5194/acp-20-3459-2020>, 2020.

- 1081 Goldberg, S. J., Carlson, C. A., Brzezinski, M., Nelson, N. B., and Siegel, D. A.: Systematic removal of neutral sugars within
1082 dissolved organic matter across ocean basins, *Geophysical Research Letters*, 38, 1–7,
1083 <https://doi.org/10.1029/2011GL048620>, 2011.
- 1084 Grawe, S., Jentsch, C., Schaefer, J., Wex, H., Mertes, S., and Stratmann, F.: Next-generation ice-nucleating particle sampling
1085 on board aircraft: characterization of the High-volume flow aERosol particle filter sAmplifier (HERA), *Atmospheric Measurement
1086 Techniques*, 16, 4551–4570, <https://doi.org/10.5194/amt-16-4551-2023>, 2023.
- 1087 Grolemond, G. and Wickham, H.: Dates and Times Made Easy with lubridate, *Journal of Statistical Software*, 40, 1–25, 2011.
- 1088 Grosse, J., Nöthig, E.-M., Torres-Valdés, S., and Engel, A.: Summertime Amino Acid and Carbohydrate Patterns in Particulate
1089 and Dissolved Organic Carbon Across Fram Strait, *Front. Mar. Sci.*, 8, <https://doi.org/10.3389/fmars.2021.684675>, 2021.
- 1090 Guo, T., Li, K., Zhu, Y., Gao, H., and Yao, X.: Concentration and size distribution of particulate oxalate in marine and coastal
1091 atmospheres – Implication for the increased importance of oxalate in nanometer atmospheric particles, *Atmospheric
1092 Environment*, 142, 19–31, <https://doi.org/10.1016/j.atmosenv.2016.07.026>, 2016.
- 1093 Gürses, Ö., Oziel, L., Karakuş, O., Sidorenko, D., Völker, C., Ye, Y., Zeising, M., Butzin, M., and Hauck, J.: Ocean biogeochemistry
1094 in the coupled ocean–sea ice–biogeochemistry model FESOM2.1–REcoM3, *Geoscientific Model Development*, 16, 4883–
1095 4936, <https://doi.org/10.5194/gmd-16-4883-2023>, 2023.
- 1096 Haddrell, A. E. and Thomas, R. J.: Aerobiology: Experimental Considerations, Observations, and Future Tools, *Appl. Environ.
1097 Microbiol.*, 83, 1–15, <https://doi.org/10.1128/AEM.00809-17>, 2017.
- 1098 Hansell, D. A.: Recalcitrant Dissolved Organic Carbon Fractions, *Annual Review of Marine Science*, 5, 421–445,
1099 <https://doi.org/10.1146/annurev-marine-120710-100757>, 2013.
- 1100 Hara, K., Yamagata, S., Yamanouchi, T., Sato, K., Herber, A., Iwasaka, Y., Nagatani, M., and Nakata, H.: Mixing states of
1101 individual aerosol particles in spring Arctic troposphere during ASTAR 2000 campaign, *Journal of Geophysical Research:
1102 Atmospheres*, 108, 1–12, <https://doi.org/10.1029/2002JD002513>, 2003.
- 1103 Hartmann, S., Schrödner, R., Hassett, B. T., Hartmann, M., van Pinxteren, M., Fomba, K. W., Stratmann, F., Herrmann, H.,
1104 Pöhlker, M., and Zeppenfeld, S.: Polysaccharides—Important Constituents of Ice-Nucleating Particles of Marine Origin,
1105 *Environ. Sci. Technol.*, 59, 5098–5108, <https://doi.org/10.1021/acs.est.4c08014>, 2025.
- 1106 Hasenecz, E., Jayarathne, T., Pendergraft, M. A., Santander, M. V., Mayer, K. J., Sauer, J., Lee, C., Gibson, W. S., Kruse, S. M.,
1107 Malfatti, F., Prather, K. A., and Stone, E. A.: Marine bacteria affect saccharide enrichment in sea spray aerosol during a
1108 phytoplankton bloom, *ACS Earth Space Chem.*, 4, 1638–1649, <https://doi.org/10.1021/acsearthspacechem.0c00167>, 2020.
- 1109 Hasenecz, E. S., Kaluarachchi, C. P., Lee, H. D., Tivanski, A. V., and Stone, E. A.: Saccharide Transfer to Sea Spray Aerosol
1110 Enhanced by Surface Activity, Calcium, and Protein Interactions, *ACS Earth Space Chem.*, 3, 2539–2548,
1111 <https://doi.org/10.1021/acsearthspacechem.9b00197>, 2019.
- 1112 Herrmann, H., Tilgner, A., Barzagli, P., Majdik, Z., Gligorovski, S., Poulain, L., and Monod, A.: Towards a more detailed
1113 description of tropospheric aqueous phase organic chemistry: CAPRAM 3.0, *Atmospheric Environment*, 39, 4351–4363,
1114 <https://doi.org/10.1016/j.atmosenv.2005.02.016>, 2005.
- 1115 Heutte, B., Bergner, N., Angot, H., Pernov, J. B., Dada, L., Mirrielees, J. A., Beck, I., Baccarini, A., Boyer, M., Creamean, J. M.,
1116 Daellenbach, K. R., El Haddad, I., Frey, M. M., Henning, S., Laurila, T., Moschos, V., Petäjä, T., Pratt, K. A., Quéléver, L. L. J.,
1117 Shupe, M. D., Zieger, P., Jokinen, T., and Schmale, J.: Observations of high-time-resolution and size-resolved aerosol chemical
1118 composition and microphysics in the central Arctic: implications for climate-relevant particle properties, *Atmospheric
1119 Chemistry and Physics*, 25, 2207–2241, <https://doi.org/10.5194/acp-25-2207-2025>, 2025.
- 1120 Hijmans, R. J.: raster: Geographic Data Analysis and Modeling, R package version 3.6-26, 2023.
- 1121 Hill, T. C. J., Malfatti, F., McCluskey, C. S., Schill, G. P., Santander, M. V., Moore, K. A., Rauker, A. M., Perkins, R. J., Celussi, M.,
1122 Levin, E. J. T., Suski, K. J., Cornwell, G. C., Lee, C., Negro, P. D., Kreidenweis, S. M., Prather, K. A., and DeMott, P. J.: Resolving
1123 the controls over the production and emission of ice-nucleating particles in sea spray, *Environ. Sci.: Atmos.*,
1124 <https://doi.org/10.1039/D2EA00154C>, 2023.
- 1125 Hoffman, E. J. and Duce, R. A.: Factors influencing the organic carbon content of marine aerosols: A laboratory study, *Journal
1126 of Geophysical Research (1896-1977)*, 81, 3667–3670, <https://doi.org/10.1029/JC081i021p03667>, 1976.
- 1127 Hogan, R. J., Mittermaier, M. P., and Illingworth, A. J.: The Retrieval of Ice Water Content from Radar Reflectivity Factor and
1128 Temperature and Its Use in Evaluating a Mesoscale Model, *Journal of Applied Meteorology and Climatology*, 45, 301–317,
1129 <https://doi.org/10.1175/JAM2340.1>, 2006.
- 1130 Hoppel, W. A., Frick, G. M., and Fitzgerald, J. W.: Surface source function for sea-salt aerosol and aerosol dry deposition to
1131 the ocean surface, *Journal of Geophysical Research: Atmospheres*, 107, AAC 7-1-AAC 7-17,
1132 <https://doi.org/10.1029/2001JD002014>, 2002.
- 1133 Illingworth, A. J., Hogan, R. J., O’Connor, E. J., Bouniol, D., Brooks, M. E., Delanoé, J., Donovan, D. P., Eastment, J. D., Gaussiat,
1134 N., Goddard, J. W. F., Haefelin, M., Baltink, H. K., Krasnov, O. A., Pelon, J., Piriou, J.-M., Protat, A., Russchenberg, H. W. J.,
1135 Seifert, A., Tompkins, A. M., Zadelhoff, G.-J. van, Vinit, F., Willén, U., Wilson, D. R., and Wrench, C. L.: Cloudnet: Continuous

- 1136 Evaluation of Cloud Profiles in Seven Operational Models Using Ground-Based Observations, *Bulletin of the American*
1137 *Meteorological Society*, 88, 883–898, <https://doi.org/10.1175/BAMS-88-6-883>, 2007.
- 1138 Ittekkot, V., Brockmann, U., Michaelis, W., and Degens, E. T.: Dissolved free and combined carbohydrates during a
1139 phytoplankton bloom in the northern North Sea, *Marine Ecology Progress Series*, 4, 299–305, 1981.
- 1140 Jayarathne, T., Sultana, C. M., Lee, C., Malfatti, F., Cox, J. L., Pendergraft, M. A., Moore, K. A., Azam, F., Tivanski, A. V., Cappa,
1141 C. D., Bertram, T. H., Grassian, V. H., Prather, K. A., and Stone, E. A.: Enrichment of Saccharides and Divalent Cations in Sea
1142 Spray Aerosol During Two Phytoplankton Blooms, *Environ Sci Technol*, 50, 11511–11520,
1143 <https://doi.org/10.1021/acs.est.6b02988>, 2016.
- 1144 Jensen, L. Z., Glasius, M., Gryning, S.-E., Massling, A., Finster, K., and Šantl-Temkiv, T.: Seasonal Variation of the Atmospheric
1145 Bacterial Community in the Greenlandic High Arctic Is Influenced by Weather Events and Local and Distant Sources, *Front.*
1146 *Microbiol.*, 13, <https://doi.org/10.3389/fmicb.2022.909980>, 2022.
- 1147 Kang, H., Jung, C. H., Lee, B. Y., Krejci, R., Heslin-Rees, D., Aas, W., and Yoon, Y. J.: Aerosol hygroscopicity influenced by
1148 seasonal chemical composition variations in the Arctic region, *Journal of Aerosol Science*, 106551,
1149 <https://doi.org/10.1016/j.jaerosci.2025.106551>, 2025.
- 1150 Kanji, Z. A., Ladino, L. A., Wex, H., Boose, Y., Burkert-Kohn, M., Cziczo, D. J., and Krämer, M.: Overview of Ice Nucleating
1151 Particles, *Meteorological Monographs*, 58, 1.1-1.33, <https://doi.org/10.1175/AMSMONOGRAPHS-D-16-0006.1>, 2017.
- 1152 Karl, M., Leck, C., Rad, F. M., Bäcklund, A., Lopez-Aparicio, S., and Heintzenberg, J.: New insights in sources of the sub-
1153 micrometre aerosol at Mt. Zeppelin observatory (Spitsbergen) in the year 2015, *Tellus B: Chemical and Physical Meteorology*,
1154 71, 1613143, <https://doi.org/10.1080/16000889.2019.1613143>, 2019.
- 1155 Kawamura, K. and Bikkina, S.: A review of dicarboxylic acids and related compounds in atmospheric aerosols: Molecular
1156 distributions, sources and transformation, *Atmospheric Research*, 170, 140–160,
1157 <https://doi.org/10.1016/j.atmosres.2015.11.018>, 2016.
- 1158 Kawamura, K., Kasukabe, H., and Barrie, L. A.: Source and reaction pathways of dicarboxylic acids, ketoacids and dicarbonyls
1159 in arctic aerosols: One year of observations, *Atmospheric Environment*, 30, 1709–1722, [https://doi.org/10.1016/1352-2310\(95\)00395-9](https://doi.org/10.1016/1352-2310(95)00395-9), 1996a.
- 1161 Kawamura, K., Sempéré, R., Imai, Y., Fujii, Y., and Hayashi, M.: Water soluble dicarboxylic acids and related compounds in
1162 Antarctic aerosols, *Journal of Geophysical Research: Atmospheres*, 101, 18721–18728, <https://doi.org/10.1029/96JD01541>,
1163 1996b.
- 1164 Keene, W. C., Pszenny, A. A. P., Galloway, J. N., and Hawley, M. E.: Sea-salt corrections and interpretation of constituent ratios
1165 in marine precipitation, *Journal of Geophysical Research*, 91, 6647–6658, <https://doi.org/10.1029/JD091iD06p06647>, 1986.
- 1166 Keene, W. C., Long, M. S., Reid, J. S., Frossard, A. A., Kieber, D. J., Maben, J. R., Russell, L. M., Kinsey, J. D., Quinn, P. K., and
1167 Bates, T. S.: Factors That Modulate Properties of Primary Marine Aerosol Generated From Ambient Seawater on Ships at Sea,
1168 *Journal of Geophysical Research: Atmospheres*, 122, 11,961-11,990, <https://doi.org/10.1002/2017JD026872>, 2017.
- 1169 Kerminen, V.-M., Teinilä, K., Hillamo, R., and Mäkelä, T.: Size-segregated chemistry of particulate dicarboxylic acids in the
1170 Arctic atmosphere, *Atmospheric Environment*, 33, 2089–2100, [https://doi.org/10.1016/S1352-2310\(98\)00350-1](https://doi.org/10.1016/S1352-2310(98)00350-1), 1999.
- 1171 Khadem, H. E.: *Carbohydrate Chemistry: Monosaccharides and Their Oligomers*, Elsevier, 267 pp., 2012.
- 1172 Kharbush, J. J., Close, H. G., Van Mooy, B. A. S., Arnosti, C., Smittenberg, R. H., Le Moigne, F. A. C., Mollenhauer, G., Scholz-
1173 Böttcher, B., Obrecht, I., Koch, B. P., Becker, K., Iversen, M. H., and Mohr, W.: Particulate Organic Carbon Deconstructed:
1174 Molecular and Chemical Composition of Particulate Organic Carbon in the Ocean, *Frontiers in Marine Science*, 7, Art.Nr. 518,
1175 <https://doi.org/10.3389/fmars.2020.00518>, 2020.
- 1176 Kirchman, D. L., Meon, B., Ducklow, H. W., Carlson, C. A., Hansell, D. A., and Steward, G. F.: Glucose fluxes and concentrations
1177 of dissolved combined neutral sugars (polysaccharides) in the Ross Sea and Polar Front Zone, Antarctica, *Deep Sea Research*
1178 *Part II: Topical Studies in Oceanography*, 48, 4179–4197, [https://doi.org/10.1016/S0967-0645\(01\)00085-6](https://doi.org/10.1016/S0967-0645(01)00085-6), 2001.
- 1179 Klein, A. M., Bohannon, B. J. M., Jaffe, D. A., Levin, D. A., and Green, J. L.: Molecular Evidence for Metabolically Active Bacteria
1180 in the Atmosphere, *Front. Microbiol.*, 7, 772, <https://doi.org/10.3389/fmicb.2016.00772>, 2016.
- 1181 Köllner, F., Schneider, J., Willis, M. D., Klimach, T., Helleis, F., Bozem, H., Kunkel, D., Hoor, P., Burkart, J., Leaitch, W. R.,
1182 Aliabadi, A. A., Abbatt, J. P. D., Herber, A. B., and Borrmann, S.: Particulate trimethylamine in the summertime Canadian high
1183 Arctic lower troposphere, *Atmospheric Chemistry and Physics*, 17, 13747–13766, [https://doi.org/10.5194/acp-17-13747-](https://doi.org/10.5194/acp-17-13747-2017)
1184 2017, 2017.
- 1185 Leck, C., Gao, Q., Mashayekhy Rad, F., and Nilsson, U.: Size-resolved atmospheric particulate polysaccharides in the high
1186 summer Arctic, *Atmospheric Chemistry and Physics*, 13, 12573–12588, <https://doi.org/10.5194/acp-13-12573-2013>, 2013.
- 1187 Leon-Marcos, A., Zeising, M., van Pinxteren, M., Zeppenfeld, S., Bracher, A., Barbaro, E., Engel, A., Feltracco, M., Tegen, I., and
1188 Heinold, B.: Modelling emission and transport of key components of primary marine organic aerosol using the global aerosol-
1189 climate model ECHAM6.3-HAM2.3, *Geoscientific Model Development*, 18, 4183–4213, [https://doi.org/10.5194/gmd-18-](https://doi.org/10.5194/gmd-18-4183-2025)
1190 4183-2025, 2025.

- 1191 Li, J., Han, Z., Fu, P., Yao, X., and Liang, M.: Seasonal characteristics of emission, distribution, and radiative effect of marine
1192 organic aerosols over the western Pacific Ocean: an investigation with a coupled regional climate aerosol model, *Atmospheric*
1193 *Chemistry and Physics*, 24, 3129–3161, <https://doi.org/10.5194/acp-24-3129-2024>, 2024.
- 1194 Lohmann, U. and Feichter, J.: Global indirect aerosol effects: a review, *Atmospheric Chemistry and Physics*, 5, 715–737,
1195 <https://doi.org/10.5194/acp-5-715-2005>, 2005.
- 1196 Macke, A. and Flores, H.: The Expeditions PS106/1 and 2 of the Research Vessel POLARSTERN to the Arctic Ocean in 2017,
1197 Bremerhaven, Germany, 171 pp., https://doi.org/10.2312/BzPM_0719_2018, 2018.
- 1198 Madry, W. L., Toon, O. B., and O’Dowd, C. D.: Modeled optical thickness of sea-salt aerosol, *Journal of Geophysical Research:*
1199 *Atmospheres*, 116, <https://doi.org/10.1029/2010JD014691>, 2011.
- 1200 Malfatti, F., Lee, C., Tinta, T., Pendergraft, M. A., Celussi, M., Zhou, Y., Sultana, C. M., Rotter, A., Axson, J. L., Collins, D. B.,
1201 Santander, M. V., Anides Morales, A. L., Aluwihare, L. I., Riemer, N., Grassian, V. H., Azam, F., and Prather, K. A.: Detection of
1202 Active Microbial Enzymes in Nascent Sea Spray Aerosol: Implications for Atmospheric Chemistry and Climate, *Environ. Sci.*
1203 *Technol. Lett.*, 6, 171–177, <https://doi.org/10.1021/acs.estlett.8b00699>, 2019.
- 1204 Manders, A. M. M., Schaap, M., Querol, X., Albert, M. F. M. A., Vercauteren, J., Kuhlbusch, T. A. J., and Hoogerbrugge, R.: Sea
1205 salt concentrations across the European continent, *Atmospheric Environment*, 44, 2434–2442,
1206 <https://doi.org/10.1016/j.atmosenv.2010.03.028>, 2010.
- 1207 Matulová, M., Husárová, S., Capek, P., Sancelme, M., and Delort, A.-M.: Biotransformation of Various Saccharides and
1208 Production of Exopolymeric Substances by Cloud-Borne Bacillus sp. 3B6, *Environ. Sci. Technol.*, 48, 14238–14247,
1209 <https://doi.org/10.1021/es501350s>, 2014.
- 1210 Maturilli, M.: Continuous meteorological observations at station Ny-Ålesund (2011-08 et seq), Alfred Wegener Institute -
1211 Research Unit Potsdam, <https://doi.org/10.1594/PANGAEA.914979>, 2020.
- 1212 Maturilli, M., Herber, A., and König-Langlo, G.: Climatology and time series of surface meteorology in Ny-Ålesund, Svalbard,
1213 *Earth System Science Data*, 5, 155–163, <https://doi.org/10.5194/essd-5-155-2013>, 2013.
- 1214 Maturilli, M., Herber, A., and König-Langlo, G.: Surface radiation climatology for Ny-Ålesund, Svalbard (78.9° N), basic
1215 observations for trend detection, *Theor Appl Climatol*, 120, 331–339, <https://doi.org/10.1007/s00704-014-1173-4>, 2015.
- 1216 Mayot, N., Matrai, P., Ellingsen, I. H., Steele, M., Johnson, K., Riser, S. C., and Swift, D.: Assessing Phytoplankton Activities in
1217 the Seasonal Ice Zone of the Greenland Sea Over an Annual Cycle, *Journal of Geophysical Research: Oceans*, 123, 8004–8025,
1218 <https://doi.org/10.1029/2018JC014271>, 2018.
- 1219 McNeill, V. F.: Aqueous Organic Chemistry in the Atmosphere: Sources and Chemical Processing of Organic Aerosols, *Environ.*
1220 *Sci. Technol.*, 49, 1237–1244, <https://doi.org/10.1021/es5043707>, 2015.
- 1221 Mirrielees, J. A., Kirpes, R. M., Costa, E. J., Porter, G. C. E., Murray, B. J., Lata, N. N., Boschi, V., China, S., Grannas, A. M., Ault,
1222 A. P., Matrai, P. A., and Pratt, K. A.: Marine aerosol generation experiments in the High Arctic during summertime, *Elementa:*
1223 *Science of the Anthropocene*, 12, 00134, <https://doi.org/10.1525/elementa.2023.00134>, 2024.
- 1224 Müller, K., Lehmann, S., Pinxteren, D. van, Gnauk, T., Niedermeier, N., Wiedensohler, A., and Herrmann, H.: Particle
1225 characterization at the Cape Verde atmospheric observatory during the 2007 RHaMBLe intensive, *Atmospheric Chemistry*
1226 *and Physics*, 10, 2709–2721, <https://doi.org/10.5194/acp-10-2709-2010>, 2010.
- 1227 Neuwirth, E.: RColorBrewer: ColorBrewer Palettes, R package version 1.1-3, 2022.
- 1228 Nomokonova, T., Ebell, K., Löhnert, U., Maturilli, M., Ritter, C., and O’Connor, E.: Statistics on clouds and their relation to
1229 thermodynamic conditions at Ny-Ålesund using ground-based sensor synergy, *Atmospheric Chemistry and Physics*, 19, 4105–
1230 4126, <https://doi.org/10.5194/acp-19-4105-2019>, 2019.
- 1231 O’Dowd, C. D. and de Leeuw, G.: Marine aerosol production: a review of the current knowledge, *Philos Trans A Math Phys*
1232 *Eng Sci*, 365, 1753–1774, <https://doi.org/10.1098/rsta.2007.2043>, 2007.
- 1233 O’Dowd, C. D., Smith, M. H., Consterdine, I. E., and Lowe, J. A.: Marine aerosol, sea-salt, and the marine sulphur cycle: a short
1234 review, *Atmospheric Environment*, 31, 73–80, [https://doi.org/10.1016/S1352-2310\(96\)00106-9](https://doi.org/10.1016/S1352-2310(96)00106-9), 1997.
- 1235 Ooki, A., Uematsu, M., Miura, K., and Nakae, S.: Sources of sodium in atmospheric fine particles, *Atmospheric Environment*,
1236 36, 4367–4374, [https://doi.org/10.1016/S1352-2310\(02\)00341-2](https://doi.org/10.1016/S1352-2310(02)00341-2), 2002.
- 1237 Orellana, M. V. and Leck, C.: Chapter 9 - Marine Microgels, in: *Biogeochemistry of Marine Dissolved Organic Matter (Second*
1238 *Edition)*, edited by: Hansell, D. A. and Carlson, C. A., Academic Press, Boston, 451–480, <https://doi.org/10.1016/B978-0-12-405940-5.00009-1>, 2015.
- 1240 Orellana, M. V., Matrai, P. A., Leck, C., Rauschenberg, C. D., Lee, A. M., and Coz, E.: Marine microgels as a source of cloud
1241 condensation nuclei in the high Arctic, *PNAS*, 108, 13612–13617, <https://doi.org/10.1073/pnas.1102457108>, 2011.
- 1242 Oziel, L., Schourup-Kristensen, V., Wekerle, C., and Hauck, J.: The Pan-Arctic Continental Slope as an Intensifying Conveyer
1243 Belt for Nutrients in the Central Arctic Ocean (1985–2015), *Global Biogeochemical Cycles*, 36, e2021GB007268,
1244 <https://doi.org/10.1029/2021GB007268>, 2022.

- 1245 Panagiotopoulos, C. and Sempéré, R.: Analytical methods for the determination of sugars in marine samples: A historical
1246 perspective and future directions, *Limnology and Oceanography: Methods*, 3, 419–454,
1247 <https://doi.org/10.4319/lom.2005.3.419>, 2005.
- 1248 Penner, J. E., Andreae, M. O., Annegarn, H., Barrie, L., Feichter, J., Hegg, D., Jayaraman, A., Leaitch, R., Murphy, D., Nganga,
1249 J., and Pitari, G.: Aerosols, their Direct and Indirect Effects, *Climate Change 2001: The Scientific Basis. Contribution of Working
1250 Group I to the Third Assessment Report of the Intergovernmental Panel on Climate Change*, 289–348, 2001.
- 1251 Pierce, D.: *ncdf4: Interface to Unidata netCDF (Version 4 or Earlier) Format Data*, R package version 1.22, 2023.
- 1252 Pilinis, C., Pandis, S. N., and Seinfeld, J. H.: Sensitivity of direct climate forcing by atmospheric aerosols to aerosol size and
1253 composition, *Journal of Geophysical Research*, 100, 18,739–18,754, <https://doi.org/10.1029/95JD02119>, 1995.
- 1254 Pilz, C., Düsing, S., Wehner, B., Müller, T., Siebert, H., Voigtländer, J., and Lonardi, M.: CAMP: an instrumented platform for
1255 balloon-borne aerosol particle studies in the lower atmosphere, *Atmospheric Measurement Techniques*, 15, 6889–6905,
1256 <https://doi.org/10.5194/amt-15-6889-2022>, 2022.
- 1257 Pilz, C., Lonardi, M., Egerer, U., Siebert, H., Ehrlich, A., Heymsfield, A. J., Schmitt, C. G., Shupe, M. D., Wehner, B., and
1258 Wendisch, M.: Profile observations of the Arctic atmospheric boundary layer with the BELUGA tethered balloon during
1259 MOSAiC, *Sci Data*, 10, 534, <https://doi.org/10.1038/s41597-023-02423-5>, 2023.
- 1260 Pilz, C., Cassano, J. J., de Boer, G., Kirbus, B., Lonardi, M., Pöhlker, M., Shupe, M. D., Siebert, H., Wendisch, M., and Wehner,
1261 B.: Tethered balloon measurements reveal enhanced aerosol occurrence aloft interacting with Arctic low-level clouds,
1262 *Elementa: Science of the Anthropocene*, 12, 00120, <https://doi.org/10.1525/elementa.2023.00120>, 2024.
- 1263 van Pinxteren, M., Müller, C., Iinuma, Y., Stolle, C., and Herrmann, H.: Chemical Characterization of Dissolved Organic
1264 Compounds from Coastal Sea Surface Microlayers (Baltic Sea, Germany), *Environmental Science & Technology*, 46, 10455–
1265 10462, <https://doi.org/10.1021/es204492b>, 2012.
- 1266 van Pinxteren, M., Barthel, S., Fomba, K. W., Müller, K., Von Tümpling, W., and Herrmann, H.: The influence of environmental
1267 drivers on the enrichment of organic carbon in the sea surface microlayer and in submicron aerosol particles – measurements
1268 from the Atlantic Ocean, *Elem Sci Anth*, 5, 1–21, <https://doi.org/10.1525/elementa.225>, 2017.
- 1269 van Pinxteren, M., Robinson, T.-B., Zeppenfeld, S., Gong, X., Bahlmann, E., Fomba, K. W., Triesch, N., Stratmann, F., Wurl, O.,
1270 Engel, A., Wex, H., and Herrmann, H.: High number concentrations of transparent exopolymer particles in ambient aerosol
1271 particles and cloud water – a case study at the tropical Atlantic Ocean, *Atmospheric Chemistry and Physics*, 22, 5725–5742,
1272 <https://doi.org/10.5194/acp-22-5725-2022>, 2022.
- 1273 van Pinxteren, M., Zeppenfeld, S., Fomba, K. W., Triesch, N., Frka, S., and Herrmann, H.: Amino acids, carbohydrates, and
1274 lipids in the tropical oligotrophic Atlantic Ocean: sea-to-air transfer and atmospheric in situ formation, *Atmospheric Chemistry
1275 and Physics*, 23, 6571–6590, <https://doi.org/10.5194/acp-23-6571-2023>, 2023.
- 1276 Platt, S. M., Hov, Ø., Berg, T., Breivik, K., Eckhardt, S., Eleftheriadis, K., Evangelidou, N., Fiebig, M., Fisher, R., Hansen, G.,
1277 Hansson, H.-C., Heintzenberg, J., Hermansen, O., Heslin-Rees, D., Holmén, K., Hudson, S., Kallenborn, R., Krejci, R., Krognes,
1278 T., Larssen, S., Lowry, D., Lund Myhre, C., Lunder, C., Nisbet, E., Nizzetto, P. B., Park, K.-T., Pedersen, C. A., Aspö Pfaffhuber,
1279 K., Röckmann, T., Schmidbauer, N., Solberg, S., Stohl, A., Ström, J., Svendby, T., Tunved, P., Tørnkvist, K., van der Veen, C.,
1280 Vratolis, S., Yoon, Y. J., Yttri, K. E., Zieger, P., Aas, W., and Tørseth, K.: Atmospheric composition in the European Arctic and
1281 30 years of the Zeppelin Observatory, Ny-Ålesund, *Atmospheric Chemistry and Physics*, 22, 3321–3369,
1282 <https://doi.org/10.5194/acp-22-3321-2022>, 2022.
- 1283 van de Poll, W. H., Maat, D. S., Fischer, P., Visser, R. J. W., Brussaard, C. P. D., and Buma, A. G. J.: Solar radiation and solar
1284 radiation driven cycles in warming and freshwater discharge control seasonal and inter-annual phytoplankton chlorophyll a
1285 and taxonomic composition in a high Arctic fjord (Kongsfjorden, Spitsbergen), *Limnology and Oceanography*, 66, 1221–1236,
1286 <https://doi.org/10.1002/lno.11677>, 2021.
- 1287 Porter, G. C. E., Adams, M. P., Brooks, I. M., Ickes, L., Karlsson, L., Leck, C., Salter, M. E., Schmale, J., Siegel, K., Sikora, S. N. F.,
1288 Tarn, M. D., Vüllers, J., Wernli, H., Zieger, P., Zinke, J., and Murray, B. J.: Highly Active Ice-Nucleating Particles at the Summer
1289 North Pole, *Journal of Geophysical Research: Atmospheres*, 127, e2021JD036059, <https://doi.org/10.1029/2021JD036059>,
1290 2022.
- 1291 Quinn, P. K., Collins, D. B., Grassian, V. H., Prather, K. A., and Bates, T. S.: Chemistry and Related Properties of Freshly Emitted
1292 Sea Spray Aerosol, *Chemical Reviews*, 115, 4383–4399, <https://doi.org/10.1021/cr500713g>, 2015.
- 1293 Ramasamy, K. P., Mahawar, L., Rajasabapathy, R., Rajeshwari, K., Miceli, C., and Pucciarelli, S.: Comprehensive insights on
1294 environmental adaptation strategies in Antarctic bacteria and biotechnological applications of cold adapted molecules, *Front.
1295 Microbiol.*, 14, <https://doi.org/10.3389/fmicb.2023.1197797>, 2023.
- 1296 Rinaldi, M., Decesari, S., Carbone, C., Finessi, E., Fuzzi, S., Ceburnis, D., O’Dowd, C. D., Sciare, J., Burrows, J. P., Vrekoussis, M.,
1297 Ervens, B., Tsigaridis, K., and Facchini, M. C.: Evidence of a natural marine source of oxalic acid and a possible link to glyoxal,
1298 *Journal of Geophysical Research: Atmospheres*, 116, <https://doi.org/10.1029/2011JD015659>, 2011.
- 1299 Robinson, T.-B., Stolle, C., and Wurl, O.: Depth is relative: the importance of depth for transparent exopolymer particles in
1300 the near-surface environment, *Ocean Science*, 15, 1653–1666, <https://doi.org/10.5194/os-15-1653-2019>, 2019a.

- 1301 Robinson, T.-B., Wurl, O., Bahlmann, E., Jürgens, K., and Stolle, C.: Rising bubbles enhance the gelatinous nature of the air–
1302 sea interface, *Limnology and Oceanography*, 64, 2358–2372, <https://doi.org/10.1002/lno.11188>, 2019b.
- 1303 Rocchi, A., von Jackowski, A., Welti, A., Li, G., Kanji, Z. A., Povozhnyy, V., Engel, A., Schmale, J., Nenes, A., Berdalet, E., Simó,
1304 R., and Dall’Osto, M.: Glucose Enhances Salinity-Driven Sea Spray Aerosol Production in Eastern Arctic Waters, *Environ. Sci.*
1305 *Technol.*, 58, 8748–8759, <https://doi.org/10.1021/acs.est.4c02826>, 2024.
- 1306 Russell, L. M., Hawkins, L. N., Frossard, A. A., Quinn, P. K., and Bates, T. S.: Carbohydrate-like composition of submicron
1307 atmospheric particles and their production from ocean bubble bursting, *Proc. Natl. Acad. Sci. U.S.A.*, 107, 6652–6657,
1308 <https://doi.org/10.1073/pnas.0908905107>, 2010.
- 1309 Sander, R., Keene, W. C., Pszenny, A. a. P., Arimoto, R., Ayers, G. P., Baboukas, E., Caine, J. M., Crutzen, P. J., Duce, R. A.,
1310 Hönniger, G., Huebert, B. J., Maenhaut, W., Mihalopoulos, N., Turekian, V. C., and Van Dingenen, R.: Inorganic bromine in
1311 the marine boundary layer: a critical review, *Atmospheric Chemistry and Physics*, 3, 1301–1336, <https://doi.org/10.5194/acp-3-1301-2003>, 2003.
- 1313 Šantl-Temkiv, T., Gosewinkel, U., Starnawski, P., Lever, M., and Finster, K.: Aeolian dispersal of bacteria in southwest
1314 Greenland: their sources, abundance, diversity and physiological states, *FEMS Microbiol Ecol*, 94,
1315 <https://doi.org/10.1093/femsec/fiy031>, 2018.
- 1316 Šantl-Temkiv, T., Amato, P., Casamayor, E. O., Lee, P. K. H., and Pointing, S. B.: Microbial ecology of the atmosphere, *FEMS*
1317 *Microbiology Reviews*, 46, fuac009, <https://doi.org/10.1093/femsre/fuac009>, 2022.
- 1318 Schartau, M., Engel, A., Schröter, J., Thoms, S., Völker, C., and Wolf-Gladrow, D.: Modelling carbon overconsumption and the
1319 formation of extracellular particulate organic carbon, *Biogeosciences*, 4, 433–454, <https://doi.org/10.5194/bg-4-433-2007>,
1320 2007.
- 1321 Schill, S. R., Burrows, S. M., Hasenecz, E. S., Stone, E. A., and Bertram, T. H.: The Impact of Divalent Cations on the Enrichment
1322 of Soluble Saccharides in Primary Sea Spray Aerosol, *Atmosphere*, 9, 476, <https://doi.org/10.3390/atmos9120476>, 2018.
- 1323 Schmale, J., Zieger, P., and Ekman, A. M. L.: Aerosols in current and future Arctic climate, *Nature Climate Change*, 11, 95–105,
1324 <https://doi.org/10.1038/s41558-020-00969-5>, 2021.
- 1325 Schmale, J., Sharma, S., Decesari, S., Pernov, J., Massling, A., Hansson, H.-C., von Salzen, K., Skov, H., Andrews, E., Quinn, P.
1326 K., Upchurch, L. M., Eleftheriadis, K., Traversi, R., Gilardoni, S., Mazzola, M., Laing, J., and Hopke, P.: Pan-Arctic seasonal cycles
1327 and long-term trends of aerosol properties from 10 observatories, *Atmospheric Chemistry and Physics*, 22, 3067–3096,
1328 <https://doi.org/10.5194/acp-22-3067-2022>, 2022.
- 1329 Sharma, S., Barrie, L. a., Magnusson, E., Brattström, G., Leaitch, W. r., Steffen, A., and Landsberger, S.: A Factor and Trends
1330 Analysis of Multidecadal Lower Tropospheric Observations of Arctic Aerosol Composition, Black Carbon, Ozone, and Mercury
1331 at Alert, Canada, *Journal of Geophysical Research: Atmospheres*, 124, 14133–14161, <https://doi.org/10.1029/2019JD030844>,
1332 2019.
- 1333 Shestakova, A., Chechin, D., Lüpkes, C., Hartmann, J., and Maturilli, M.: Foehn effect during easterly flow over Svalbard,
1334 <https://doi.org/10.5194/acp-2021-478>, 2021.
- 1335 Simon, D. J., Hartmann, J., Schaefer, J., Zeppenfeld, S., Lüpkes, C., Hartmann, M., Wetzel, B., Heinold, B., Jurányi, Z., Schulz,
1336 A., Köhler, L., Jörss, A.-M., Herber, A., Henning, S., Pöhlker, M. L., Roberts, G. C., and Stratmann, F.: Turbulent aerosol fluxes
1337 from airborne measurements over the Arctic Ocean, *Geophys. Res. Lett.*, 52, e2025GL117094,
1338 <https://doi.org/10.1029/2025GL117094>, 2025
- 1339 Sinreich, R., Coburn, S., Dix, B., and Volkamer, R.: Ship-based detection of glyoxal over the remote tropical Pacific Ocean,
1340 *Atmospheric Chemistry and Physics*, 10, 11359–11371, <https://doi.org/10.5194/acp-10-11359-2010>, 2010.
- 1341 Sorooshian, A., Lu, M.-L., Brechtel, F. J., Jonsson, H., Feingold, G., Flagan, R. C., and Seinfeld, J. H.: On the Source of Organic
1342 Acid Aerosol Layers above Clouds, *Environ. Sci. Technol.*, 41, 4647–4654, <https://doi.org/10.1021/es0630442>, 2007.
- 1343 Stein, A. F., Draxler, R. R., Rolph, G. D., Stunder, B. J. B., Cohen, M. D., and Ngan, F.: NOAA’s HYSPLIT Atmospheric Transport
1344 and Dispersion Modeling System, *Bull. Amer. Meteor. Soc.*, 96, 2059–2077, <https://doi.org/10.1175/BAMS-D-14-00110.1>,
1345 2015.
- 1346 Struthers, H., Ekman, A. M. L., Glantz, P., Iversen, T., Kirkevåg, A., Mårtensson, E. M., Seland, Ø., and Nilsson, E. D.: The effect
1347 of sea ice loss on sea salt aerosol concentrations and the radiative balance in the Arctic, *Atmospheric Chemistry and Physics*,
1348 11, 3459–3477, <https://doi.org/10.5194/acp-11-3459-2011>, 2011.
- 1349 Su, B., Bi, X., Zhang, Z., Liang, Y., Song, C., Wang, T., Hu, Y., Li, L., Zhou, Z., Yan, J., Wang, X., and Zhang, G.: Enrichment of
1350 calcium in sea spray aerosol: insights from bulk measurements and individual particle analysis during the R/V *Xuelong* cruise
1351 in the summertime in Ross Sea, Antarctica, *Atmospheric Chemistry and Physics*, 23, 10697–10711,
1352 <https://doi.org/10.5194/acp-23-10697-2023>, 2023.
- 1353 Theodosi, C., Im, U., Bougiatioti, A., Zarpas, P., Yenigun, O., and Mihalopoulos, N.: Aerosol chemical composition over
1354 Istanbul, *Science of The Total Environment*, 408, 2482–2491, <https://doi.org/10.1016/j.scitotenv.2010.02.039>, 2010.

- 1355 Thyng, K., Greene, C. A., Hetland, R. D., Zimmerle, H. M., and DiMarco, S.: True colors of oceanography: Guidelines for effective
1356 and accurate colormap selection, *Oceanography*, 3, <https://doi.org/10.5670/oceanog.2016.66>, 2016.
- 1357 Tilgner, A. and Herrmann, H.: Radical-driven carbonyl-to-acid conversion and acid degradation in tropospheric aqueous
1358 systems studied by CAPRAM, *Atmospheric Environment*, 44, 5415–5422, <https://doi.org/10.1016/j.atmosenv.2010.07.050>,
1359 2010.
- 1360 Tørseth, K., Aas, W., Breivik, K., Fjæraa, A. M., Fiebig, M., Hjellbrekke, A. G., Lund Myhre, C., Solberg, S., and Yttri, K. E.:
1361 Introduction to the European Monitoring and Evaluation Programme (EMEP) and observed atmospheric composition change
1362 during 1972–2009, *Atmospheric Chemistry and Physics*, 12, 5447–5481, <https://doi.org/10.5194/acp-12-5447-2012>,
1363 2012.
- 1364 Trainic, M., Koren, I., Sharoni, S., Frada, M., Segev, L., Rudich, Y., and Vardi, A.: Infection Dynamics of a Bloom-Forming Alga
1365 and Its Virus Determine Airborne Coccolith Emission from Seawater, *iScience*, 6, 327–335,
1366 <https://doi.org/10.1016/j.isci.2018.07.017>, 2018.
- 1367 Triesch, N., van Pinxteren, M., Engel, A., and Herrmann, H.: Concerted measurements of free amino acids at the Cabo Verde
1368 islands: high enrichments in submicron sea spray aerosol particles and cloud droplets, *Atmospheric Chemistry and Physics*,
1369 21, 163–181, <https://doi.org/10.5194/acp-21-163-2021>, 2021.
- 1370 Turekian, V. C., Macko, S. A., and Keene, W. C.: Concentrations, isotopic compositions, and sources of size-resolved,
1371 particulate organic carbon and oxalate in near-surface marine air at Bermuda during spring, *Journal of Geophysical Research:*
1372 *Atmospheres*, 108, <https://doi.org/10.1029/2002JD002053>, 2003.
- 1373 Veron, F.: Ocean Spray, *Annual Review of Fluid Mechanics*, 47, 507–538, <https://doi.org/10.1146/annurev-fluid-010814-014651>, 2015.
- 1375 Vihtakari, M.: PlotSvalbard: PlotSvalbard-Plot research data from Svalbard on maps, R package version 0.9 2, 2020.
- 1376 Warneck, P.: In-cloud chemistry opens pathway to the formation of oxalic acid in the marine atmosphere, *Atmospheric*
1377 *Environment*, 37, 2423–2427, [https://doi.org/10.1016/S1352-2310\(03\)00136-5](https://doi.org/10.1016/S1352-2310(03)00136-5), 2003.
- 1378 Wendisch, M., Brückner, M., Burrows, J. P., Crewell, S., Dethloff, K., Ebell, K., Lüpkes, C., Macke, A., Notholt, J., and Quaas, J.:
1379 Understanding causes and effects of rapid warming in the Arctic, *Eos*, 98, 2017.
- 1380 Wendisch, M., Macke, A., Ehrlich, A., Lüpkes, C., Mech, M., Chechin, D., Dethloff, K., Barrientos, C., Bozem, H., Brückner, M.,
1381 Clemen, H.-C., Crewell, S., Donth, T., Dupuy, R., Ebell, K., Egerer, U., Engelmann, R., Engler, C., Eppers, O., Gehrmann, M.,
1382 Gong, X., Gottschalk, M., Gourbeyre, C., Griesche, H., Hartmann, J., Hartmann, M., Heinold, B., Herber, A., Herrmann, H.,
1383 Heygster, G., Hoor, P., Jafariserajehlou, S., Jäkel, E., Järvinen, E., Jourdan, O., Kästner, U., Kecorius, S., Knudsen, E. M., Köllner,
1384 F., Kretzschmar, J., Lelli, L., Leroy, D., Maturilli, M., Mei, L., Mertes, S., Mioche, G., Neuber, R., Nicolaus, M., Nomokonova, T.,
1385 Notholt, J., Palm, M., van Pinxteren, M., Quaas, J., Richter, P., Ruiz-Donoso, E., Schäfer, M., Schmieder, K., Schnaiter, M.,
1386 Schneider, J., Schwarzenböck, A., Seifert, P., Shupe, M. D., Siebert, H., Spreen, G., Stapf, J., Stratmann, F., Vogl, T., Welti, A.,
1387 Wex, H., Wiedensohler, A., Zannata, M., and Zeppenfeld, S.: The Arctic Cloud Puzzle: Using ALOUD/PASCAL Multi-Platform
1388 Observations to Unravel the Role of Clouds and Aerosol Particles in Arctic Amplification, *Bull. Amer. Meteor. Soc.*,
1389 <https://doi.org/10.1175/BAMS-D-18-0072.1>, 2018.
- 1390 Wendisch, M., Brückner, M., Crewell, S., Ehrlich, A., Notholt, J., Lüpkes, C., Macke, A., Burrows, J. P., Rinke, A., Quaas, J.,
1391 Maturilli, M., Schemann, V., Shupe, M. D., Akansu, E. F., Barrientos-Velasco, C., Bärfuss, K., Blechschmidt, A.-M., Block, K.,
1392 Bougoudis, I., Bozem, H., Böckmann, C., Bracher, A., Bresson, H., Bretschneider, L., Buschmann, M., Chechin, D. G., Chylik, J.,
1393 Dahlke, S., Deneke, H., Dethloff, K., Donth, T., Dorn, W., Dupuy, R., Ebell, K., Egerer, U., Engelmann, R., Eppers, O., Gerdes, R.,
1394 Gierens, R., Gorodetskaya, I. V., Gottschalk, M., Griesche, H., Gryanik, V. M., Handorf, D., Harm-Altstädter, B., Hartmann, J.,
1395 Hartmann, M., Heinold, B., Herber, A., Herrmann, H., Heygster, G., Höschel, I., Hofmann, Z., Hölemann, J., Hünerbein, A.,
1396 Jafariserajehlou, S., Jäkel, E., Jacobi, C., Janout, M., Jansen, F., Jourdan, O., Jurányi, Z., Kalesse-Los, H., Kanzow, T., Käthner,
1397 R., Kliesch, L. L., Klingebiel, M., Knudsen, E. M., Kovács, T., Körtke, W., Krampe, D., Kretzschmar, J., Kreyling, D., Kulla, B.,
1398 Kunkel, D., Lampert, A., Lauer, M., Lelli, L., Lerber, A. von, Linke, O., Löhnert, U., Lonardi, M., Losa, S. N., Losch, M., Maahn,
1399 M., Mech, M., Mei, L., Mertes, S., Metzner, E., Mewes, D., Michaelis, J., Mioche, G., Moser, M., Nakoudi, K., Neggers, R.,
1400 Neuber, R., Nomokonova, T., Oelker, J., Papakonstantinou-Presvelou, I., et al.: Atmospheric and Surface Processes, and
1401 Feedback Mechanisms Determining Arctic Amplification: A Review of First Results and Prospects of the (AC)3 Project, *Bulletin*
1402 *of the American Meteorological Society*, 104, E208–E242, <https://doi.org/10.1175/BAMS-D-21-0218.1>, 2023.
- 1403 White, W. H.: Chemical markers for sea salt in IMPROVE aerosol data, *Atmospheric Environment*, 42, 261–274,
1404 <https://doi.org/10.1016/j.atmosenv.2007.09.040>, 2008.
- 1405 Wickham, H.: Reshaping Data with the reshape Package, *Journal of Statistical Software*, 21, 1–20, 2007.
- 1406 Wickham, H.: ggplot2: Elegant Graphics for Data Analysis, Springer-Verlag New York, https://doi.org/10.1007/978-3-319-24277-4_2, 2016.
- 1408 Wickham, H., François, R., Henry, L., Müller, K., and Vaughan, D.: dplyr: A Grammar of Data Manipulation, R package version
1409 1.1.4, 2023a.
- 1410 Wickham, H., Pedersen, T. L., and Seidel, D.: scales: Scale Functions for Visualization, R package version 1.3.0, 2023b.

- 1411 Wietz, M., Engel, A., Ramondenc, S., Niwano, M., von Appen, W.-J., Priest, T., von Jackowski, A., Metfies, K., Bienhold, C., and
1412 Boetius, A.: The Arctic summer microbiome across Fram Strait: Depth, longitude, and substrate concentrations structure
1413 microbial diversity in the euphotic zone, *Environmental Microbiology*, 26, e16568, <https://doi.org/10.1111/1462-2920.16568>, 2024.
- 1415 Wietz, M., van Pinxteren, M., Freese, H. M., Sproer, C., and Zeppenfeld, S.: Seasonal connectivity of microbes and
1416 carbohydrates between ocean, atmosphere, and cryosphere in Kongsfjorden (Svalbard, Arctic Ocean), preprint,
1417 <https://doi.org/10.64898/2025.12.01.691664>, uploaded on 2 December 2025.
- 1418 Willis, M. D., Leaitch, W. R., and Abbatt, J. P. D.: Processes Controlling the Composition and Abundance of Arctic Aerosol,
1419 *Reviews of Geophysics*, 56, 621–671, <https://doi.org/10.1029/2018RG000602>, 2018.
- 1420 Wong, J. P. S., Tsagkaraki, M., Tsiodra, I., Mihalopoulos, N., Violaki, K., Kanakidou, M., Sciare, J., Nenes, A., and Weber, R. J.:
1421 Effects of Atmospheric Processing on the Oxidative Potential of Biomass Burning Organic Aerosols, *Environ. Sci. Technol.*, 53,
1422 6747–6756, <https://doi.org/10.1021/acs.est.9b01034>, 2019.
- 1423 Wurl, O. and Holmes, M.: The gelatinous nature of the sea-surface microlayer, *Marine Chemistry*, 110, 89–97,
1424 <https://doi.org/10.1016/j.marchem.2008.02.009>, 2008.
- 1425 Xu, W., Ovadnevaite, J., Fossum, K. N., Lin, C., Huang, R.-J., Ceburnis, D., and O’Dowd, C.: Sea spray as an obscured source for
1426 marine cloud nuclei, *Nat. Geosci.*, 15, 282–286, <https://doi.org/10.1038/s41561-022-00917-2>, 2022.
- 1427 Yang, C., Zhou, S., Zhang, C., Yu, M., Cao, F., and Zhang, Y.: Atmospheric Chemistry of Oxalate: Insight Into the Role of Relative
1428 Humidity and Aerosol Acidity From High-Resolution Observation, *Journal of Geophysical Research: Atmospheres*, 127,
1429 e2021JD035364, <https://doi.org/10.1029/2021JD035364>, 2022.
- 1430 Yttri, K. E., Bäcklund, A., Conen, F., Eckhardt, S., Evangeliou, N., Fiebig, M., Kasper-Giebl, A., Gold, A., Gundersen, H., Myhre,
1431 C. L., Platt, S. M., Simpson, D., Surratt, J. D., Szidat, S., Rauber, M., Tørseth, K., Ytre-Eide, M. A., Zhang, Z., and Aas, W.:
1432 Composition and sources of carbonaceous aerosol in the European Arctic at Zeppelin Observatory, Svalbard (2017 to 2020),
1433 *Atmospheric Chemistry and Physics*, 24, 2731–2758, <https://doi.org/10.5194/acp-24-2731-2024>, 2024.
- 1434 Yu, H., Kaufman, Y. J., Chin, M., Feingold, G., Remer, L. A., Anderson, T. L., Balkanski, Y., Bellouin, N., Boucher, O., Christopher,
1435 S., DeCola, P., Kahn, R., Koch, D., Loeb, N., Reddy, M. S., Schulz, M., Takemura, T., and Zhou, M.: A review of measurement-
1436 based assessments of the aerosol direct radiative effect and forcing, *Atmospheric Chemistry and Physics*, 6, 613–666,
1437 <https://doi.org/10.5194/acp-6-613-2006>, 2006.
- 1438 Zäncker, B., Cunliffe, M., and Engel, A.: Eukaryotic community composition in the sea surface microlayer across an east–west
1439 transect in the Mediterranean Sea, *Biogeosciences*, 18, 2107–2118, <https://doi.org/10.5194/bg-18-2107-2021>, 2021.
- 1440 Zeising, M., Oziel, L., Thoms, S., Gürses, Ö., Hauck, J., Heinold, B., Losa, S. N., van Pinxteren, M., Völker, C., Zeppenfeld, S., and
1441 Bracher, A.: Assessment of transparent exopolymer particles in the Arctic Ocean implemented into the coupled ocean–sea
1442 ice–biogeochemistry model FESOM2.1–REcoM3, *Geoscientific Model Development*, 19, 2077–2109,
1443 <https://doi.org/10.5194/gmd-19-2077-2026>, 2026.
- 1444 Zeppenfeld, S. and Schmidt, L.: Dissolved and particulate carbohydrates and inorganic ions in the sea surface microlayer and
1445 bulk water of Kongsfjorden (Autumn 2021/Spring 2022), <https://doi.org/10.1594/PANGAEA.982606>, 2025.
- 1446 Zeppenfeld, S., van Pinxteren, M., Engel, A., and Herrmann, H.: A protocol for quantifying mono- and polysaccharides in
1447 seawater and related saline matrices by electro-dialysis (ED) – combined with HPAEC-PAD, *Ocean Science*, 16, 817–830,
1448 <https://doi.org/10.5194/os-16-817-2020>, 2020.
- 1449 Zeppenfeld, S., van Pinxteren, M., van Pinxteren, D., Wex, H., Berdalet, E., Vaqué, D., Dall’Osto, M., and Herrmann, H.: Aerosol
1450 Marine Primary Carbohydrates and Atmospheric Transformation in the Western Antarctic Peninsula, *ACS Earth Space Chem.*,
1451 5, 1032–1047, <https://doi.org/10.1021/acsearthspacechem.0c00351>, 2021.
- 1452 Zeppenfeld, S., van Pinxteren, M., Hartmann, M., Zeising, M., Bracher, A., and Herrmann, H.: Marine carbohydrates in Arctic
1453 aerosol particles and fog – diversity of oceanic sources and atmospheric transformations, *Atmospheric Chemistry and Physics*,
1454 23, 15561–15587, <https://doi.org/10.5194/acp-23-15561-2023>, 2023.
- 1455 Zeppenfeld, S., Schaefer, J., van Pinxteren, M., and Schmidt, L.: Marine combined carbohydrates and inorganic ions in
1456 atmospheric total suspended particles across altitudes in the lower troposphere of Ny-Ålesund, Svalbard,
1457 <https://doi.org/10.1594/PANGAEA.982703>, 2025.
- 1458 Zhou, S., Gonzalez, L., Leithead, A., Finewax, Z., Thalman, R., Vlasenko, A., Vagle, S., Miller, L. A., Li, S.-M., Bureekul, S.,
1459 Furutani, H., Uematsu, M., Volkamer, R., and Abbatt, J.: Formation of gas-phase carbonyls from heterogeneous oxidation of
1460 polyunsaturated fatty acids at the air–water interface and of the sea surface microlayer, *Atmospheric Chemistry and Physics*,
1461 14, 1371–1384, <https://doi.org/10.5194/acp-14-1371-2014>, 2014.
- 1462 Zhu, B., Sun-Waterhouse, D., and You, L.: Insights into the mechanisms underlying the degradation of xylooligosaccharides in
1463 UV/H₂O₂ system, *Carbohydrate Polymers*, 317, 121091, <https://doi.org/10.1016/j.carbpol.2023.121091>, 2023.

1464 Zhu, Y.-S., Connolly, A., Guyon, A., and FitzGerald, R. J.: Solubilisation of calcium and magnesium from the marine red algae
1465 *Lithothamnion calcareum*, *International Journal of Food Science and Technology*, 49, 1600–1606,
1466 <https://doi.org/10.1111/ijfs.12459>, 2014.